Atmos. Chem. Phys. Discuss., 13, 4727–4784, 2013
www.atmos-chem-phys-discuss.net/13/4727/2013/
doi:10.5194/acpd-13-4727-2013

Atmospheric Chemistry and Physics Discussions

The seasonal vertical distribution of the Saharan Air Layer and its modulation by the wind

C. Tsamalis[1], A. Chédin[1], J. Pelon[2], and V. Capelle[1]

[1]Laboratoire de Météorologie Dynamique, UMR8539, CNRS – IPSL, Ecole Polytechnique, Palaiseau, France
[2]UPMC Univ. Paris 06, UMR8190, CNRS/INSU – Université Versailles St-Quentin, LATMOS-IPSL, Paris, France

Received: 1 February 2013 – Accepted: 5 February 2013 – Published: 19 February 2013

Correspondence to: C. Tsamalis (christoforos.tsamalis@gmail.com)

Published by Copernicus Publications on behalf of the European Geosciences Union.

Abstract

The Saharan Air Layer (SAL) influences large scale environment from West Africa to eastern tropical America, by carrying large amounts of dust aerosols. However, the vertical distribution of the SAL is not well established due to a lack of systematic measurements away from the continents. This can be overcome by using the observations of the space lidar CALIOP on board CALIPSO. By taking advantage of CALIOP capability to distinguish dust aerosols from other types of aerosols through depolarization, the seasonal vertical distribution of the SAL is analysed at 1 degree horizontal resolution over a period of 5 yr (June 2006–May 2011). This study shows that SAL can be identified all year round displaying a clear seasonal cycle. It occurs higher in altitude and more northern in latitude during summer than during winter, but with similar latitude extent near Africa for the four seasons. The south border of the SAL is determined by the Intertropical Convergence Zone (ITCZ), which either prohibits dust layers to penetrate it or reduces significantly the number of dust layers seen in or south of it, as over the eastern tropical Atlantic. Spatially, near Africa, it is found between 5° S–15° N in winter going at 5–30° N in summer. Towards America (50° W), SAL is observed between 5° S–10° N in winter and 10–25° N in summer. During spring and fall, SAL is found between the position of winter and summer not only spatially, but also vertically. In winter, SAL occurs in the altitude range 0–3 km off West Africa, decreasing to 0–2 km close to South America. During summer, SAL is found to be thicker and higher near Africa at 1–5 km, reducing to 0–2 km in the Gulf of Mexico, farther west than during the other seasons. SAL is confined to one layer, of which the mean altitude is decreasing with westward transport by 13 m deg^{-1} during winter and 28 m deg^{-1}, after 30° W, during summer. Its mean geometrical thickness is decreasing by 25 m deg^{-1} in winter and 9 m deg^{-1} in summer. Spring and fall present similar characteristics for both mean altitude and geometrical thickness. Wind plays a major role not only for the transport of dust within the SAL, but also by sculpting it. During winter, the trade winds transport SAL towards South America, while in spring and summer they scavenge dust

ACPD
13, 4727–4784, 2013

aerosols below it by bringing maritime air masses from North Atlantic up to about 50° W. The North Atlantic westerlies, with their southern border occurring between 15° N and 30° N (depending on the season, the longitude and the altitude), prevent the SAL to develop further northward. In addition, their southward shift with altitude gives SAL its characteristic oval shape in the northern part. The effective dry deposition velocity of dust particles is estimated to be 0.07–0.08 cm s^{-1} in winter, 0.13–0.15 cm s^{-1} in spring and fall, and 0.2 cm s^{-1} in summer. Finally, the African Easterly Jet (AEJ) is observed to collocate with the maximum dust load of the SAL and this might promote the differential advection for SAL parts, especially during summer.

1 Introduction

It is well known that large quantities of Saharan dust are transported across the tropical Atlantic throughout the year as a result of large-scale Saharan dust outbreaks, with the maximum occurring during summer. These dust outbreaks are mostly confined to a deep mixed layer, commonly referred to as the Saharan Air Layer (SAL), that can reach North America during summer and South America during winter. SAL is not only characterized by its load in dust aerosols, but also by dry and warm air (Dunion and Marron, 2008). The SAL long range transport is enhanced by the persistent temperature inversions that exist at its base and top, in part because of the interaction of dust aerosols with radiation, thus keeping the SAL relatively warm and stable as it crosses Atlantic (Karyampudi et al., 1999). However, both the dust and low humidity are essential to maintaining the temperature structure in the SAL against thermal relaxation (Wong et al., 2009).

SAL, due to its load of dust aerosols, influences in many ways the tropical environment from West Africa to America. The interaction of dust with radiation through scattering and absorption in the visible and thermal infrared spectra heats the lower atmosphere within the dust layer over the tropical Atlantic Ocean (Alpert et al., 1998; Wang, 2009; Davidi et al., 2012), thus affecting locally the radiative budget and modifying the

ACPD
13, 4727–4784, 2013

atmospheric stability. Simultaneously, the impact of dust on radiation affects the ocean temperature over tropical Atlantic on interannual to decadal timescales (Evan et al., 2009, 2011). A robust negative correlation between atmospheric dust loading and Atlantic sea surface temperature is found, consistent with the notion that increased (decreased) Saharan dust is associated with cooling (warming) of the Atlantic during the early hurricane season (July to September) (Lau and Kim, 2007). Wu (2007) found also an anti-correlation between SAL activity and hurricane intensity, while other studies reported that SAL can suppress tropical cyclogenesis (Evan et al., 2006; Jenkins et al., 2008). The tropical cyclone genesis and development may be affected by the enhancement of the vertical shear, which takes place to the south of the SAL due to dust-radiation effects (Chen et al., 2010). During the last years the connection of SAL with the activity of tropical cyclones has become an active research area (Dunion and Velden, 2004; Sun et al., 2008; Zipser et al., 2009) because of their strong socio-economical impacts. However, a recent study noticed that the SAL is not a determinant factor of intensity for tropical cyclones (Braun, 2010), although the dust impacts have not been taken into account. On the other hand, SAL suppresses convection over the eastern and central tropical North Atlantic (Wong and Dessler, 2005), where the dust load is important.

Further, SAL can shift rainfall northward by 1 to 4 degrees along the Intertropical Convergence Zone (ITCZ) (Wilcox et al., 2010). In addition, Saharan dust may serve as cloud condensation nuclei or ice nuclei, affecting cloud microphysics and decreasing precipitation (DeMott et al., 2003; Mahowald and Kiehl, 2003; Twohy et al., 2009). During dust events, the concentration of trace gases, like ozone, nitrogen oxides and organic radicals, is reduced due to heterogeneous reactions on dust aerosols (de Reus et al., 2005; Jenkins et al., 2012), thus changing the oxidizing capacity of the atmosphere. Besides, SAL dust aerosols fertilize large areas of Atlantic Ocean and Amazon Basin by transport and deposition of nutrients, like iron and phosphorus, which in turn may impact many biogeochemical cycles (Jickells et al., 2005; Kaufman et al., 2005;

ACPD
13, 4727–4784, 2013

Bristow et al., 2010). It should be noted that the deposition rates strongly depend on the vertical dust distribution, which varies with seasons (Schepanski et al., 2009).

The SAL has been studied at dedicated sites with observations at both sides of the tropical Atlantic (e.g. Chiapello et al., 1995; Prospero and Lamb, 2003), during specific campaigns (e.g. Reid et al., 2002; Ansmann et al., 2009) or using space observations (e.g. Zhu et al., 2007; Doherty et al., 2008). However, local measurements do not offer a global and complete view of dust outbreaks, due to the lack of systematic measurements away from the continents. The same holds for campaigns, by definition limited in time, although they provide a plethora of observations at regional scale. Satellite observations can describe the whole phenomenon on a daily basis, offering an almost global coverage (depending on the swath width). Nevertheless, the retrieval from space of thermodynamic variables, like temperature, is affected by the presence of dust (Zhang and Zhang, 2008; Maddy et al., 2012). On the other hand, aerosol satellite measurements in the solar spectrum mostly provide column integrated properties like the optical depth, without information about the vertical distribution. Indeed, the vertical global structure of the SAL has been paid little attention, in part due to the lack of available measurements before the CALIPSO mission. However, the vertical distribution of dust aerosols is a key parameter for the radiative forcing, both in solar and terrestrial spectra (Liao and Seinfeld, 1998; Meloni et al., 2005; Shell and Somerville, 2007). In addition, the dust satellite observations are sensitive to the vertical distribution, especially in the ultraviolet and infrared spectra, which renders the retrieval of dust characteristics from space more challenging (Quijano et al., 2000; Ginoux and Torres, 2003; Pierangelo et al., 2004; Torres et al., 2007). At the same time, this sensitivity permits to new generation infrared sounders to bring reliable information on the dust layer mean altitude (Peyridieu et al., 2010, 2012), but their new established results still need further validation. An accurate determination of the aerosol vertical distribution at global scale can be achieved with the two-wavelength polarization sensitive lidar CALIOP, launched on board CALIPSO in April 2006 (Winker et al., 2007).

ACPD
13, 4727–4784, 2013

Recent studies using CALIPSO data examined the vertical structure of SAL, but these were either case studies (e.g. Liu et al., 2008b; Ben-Ami et al., 2010), thus restricted in time, or climatological studies (Generoso et al., 2008; Liu et al., 2008a; Ben-Ami et al., 2009; Braun, 2010; Yu et al., 2010; Adams et al., 2012; Ridley et al., 2012; Yang et al., 2012), restricted to the description of dust vertical distribution by presenting means at regional scale using mainly previous versions of CALIPSO data, which showed significant errors regarding the discrimination between clouds and aerosols, or less focused. Here, the seasonal vertical distribution of the SAL at 1° spatial resolution is presented based on 5 yr of CALIPSO observations, bringing a more detailed description of its spatial structure at a relatively fine scale. Furthermore, the CALIPSO aerosol types desert dust and polluted dust are combined to avoid the potential misclassification of desert dust aerosols as polluted dust in the algorithm. This combination allows also to better account for ageing of dust aerosols with transport. Also here, data from ECMWF reanalysis are used in order to examine the influence of wind on the SAL shape. Data and method are described in Sect. 2. Section 3 presents the vertical distribution of the SAL. The connection between SAL and wind is presented in Sect. 4 and finally summary and conclusions are given in Sect. 5.

2 Data

2.1 CALIPSO data and methodology

CALIOP provides data since June 2006 and it is the primary instrument onboard CALIPSO, which is part of the "A-Train" constellation of satellites. This space lidar is based on a Nd : YAG laser measuring the backscatter signal at 532 nm and 1064 nm and the degree of linear polarization at 532 nm. CALIOP observes aerosols and clouds with high vertical resolution of 30–60 m (up to 20 km) during its 16-day repeat cycle, while its beam diameter is about 70 m at the Earth surface (Winker et al., 2007). Winker et al. (2009) provide an overview of CALIPSO data products and of the algorithms used

ACPD
13, 4727–4784, 2013

to produce them. In this study, we use CALIPSO level 2 data, the 5 km aerosol layer product, version 3.01, above the Atlantic for the 5-yr period June 2006–May 2011.

In CALIOP data, the layer (aerosol or cloud) boundaries are identified with a multiscale retrieval approach in order to achieve an optimum balance between signal to noise ratio and spatial resolution (Vaughan et al., 2009). The aerosol layer product is reported at the resolution of 5 km, which is not always equal to the detection resolution (0.333, 1, 5, 20 or 80 km). The signal of layers detected at finer resolution is removed before moving on to further averaging. However, layers detected with finer resolution may appear to overwrite or overlap in the vertical dimension with layers found at coarser resolution. In order to avoid counting several times the same layer, this overwriting has been corrected. When in a column of 5 km two or more layers appear to overlap, the top is defined as the maximum top altitude of the overlapping layers and respectively the bottom as the minimum base altitude of the layers. A similar correction has been applied by Thorsen et al. (2011) in the case of cirrus clouds. Figure 1 presents an example of CALIOP signal cross section (top) above the Atlantic. The triangles show the boundaries of dust layers (see below for their definition) as detected by CALIPSO algorithms, while the white lines indicate the overlap.

Afterwards, CALIPSO discriminates between clouds and aerosols, based on statistical differences in their optical and physical properties by using 5-dimensional probability distribution functions in version 3 (Liu et al., 2009, 2010). The confidence level of discrimination is provided by the cloud-aerosol discrimination (CAD) score, which ranges from −100 to 100, with negative values indicating aerosols and high absolute value meaning high confidence. Here, only aerosol layers with high confidence of discrimination are used with Feature Type Quality Assessment (QA) = 3, meaning CAD score ≤ -70. It should be mentioned that some misclassification of dust aerosols as clouds (mostly cirrus) may still occur in the case of moderately dense dust plumes transported to high latitudes or to high altitudes even at low latitudes. This happens very rarely over the ocean, and high resolution can be helpful to improve misclassifications.

ACPD
13, 4727–4784, 2013

Once the layer has been identified as aerosol, then an algorithm classifies it as one of the six defined types: desert dust, smoke, clean continental, polluted continental, clean marine and polluted dust (Omar et al., 2009). CALIOP using depolarisation at 532 nm, is able to discriminate between dust and other types of aerosols (smoke, continental, marine), which generally do not depolarize light as they are mainly spherical (e.g. Iwasaka et al., 2003; Ansmann et al., 2009; Winker et al., 2010). Indeed, the better identification of dust aerosols in comparison to other types from CALIOP has been confirmed with AERONET measurements, with agreement percentages of 91 % and 53 % for dust and polluted dust aerosol types, respectively (Mielonen et al., 2009). Polluted dust corresponds to low depolarization values (< 20 %) and this type of aerosol is detected about 20 % of the time (Omar et al., 2009). There are however some misclassification issues, and polluted dust is expected to be identified too often (D. Winker, personal communication, 2012).

In order to take into account the possible change of dust aerosol properties with transport, the two CALIPSO types desert dust and polluted dust are thus combined in our analysis, with their sum stated as dust for the rest of the study. Indeed, after their emission from North Africa, dust aerosols can be mixed with other types of aerosols like biomass burning or anthropogenic pollution and then transported further away (Ansmann et al., 2009; Rodriguez et al., 2011). On the other hand, above the ocean they can be mixed with maritime aerosols (Knippertz et al., 2011; Yang et al., 2012). Also, dust aerosols can uptake trace gases on their surface (Andreae and Crutzen, 1997; Formenti et al., 2011), thus changing their composition and finally their optical characteristics. Away from Sahara, the inclusion of polluted dust layers may alter the results because of the non-desert origin of some of these layers. Consequently, away from Sahara and close to biomass burning or pollution sources, like over Africa and South America, results are treated with caution and, as far as possible this is discussed in this paper and a statement is issued. The good quality of dust detection from the CALIPSO algorithms can be observed in Fig. 1, where an example of SAL is presented. CALIPSO captures adequately the top and the base of the dust layers (indicated by the triangles),

ACPD
13, 4727–4784, 2013

while it avoids the misclassification of dust as cloud and conversely (clouds are shown as dark brown features).

CALIOP as a lidar has a very small swath width, while the distance between two successive CALIPSO tracks is more than 2000 km in the low and mid-latitudes. As a result, a considerable averaging in space and in time is required for producing statistically meaningful results (Winker et al., 2010). Here, seasonal means with 1° resolution are calculated using the first 5 yr of CALIOP available observations, including both nighttime and daytime data. The nighttime data have better signal to noise ratio (Wu et al., 2011) and this is reflected in the percentage of daytime layers to the total number of layers which is about 30 %. In order to ensure a minimum level of statistical significance, the number of at least 240 layers is imposed to every bin of 1°.

In order to avoid the dependence of the results on the lidar ratio, which is ill-constrained by CALIOP as an elastic lidar, the occurrence frequency is used instead. The lidar ratio for dust aerosols can vary significantly between 20 and 100 sr (Mattis et al., 2002; Balis et al., 2004), while statistical studies indicate values mostly between 30 and 70 sr (Cattrall et al., 2005; Muller et al., 2007). Different dust source regions have distinct lidar ratios (Muller et al., 2007), while even within Sahara the variability of lidar ratio is significant (Schuster et al., 2012). In CALIPSO algorithm the lidar ratio at 532 nm for desert dust is set to 40 sr and to 55 sr for polluted dust aerosols (it was 65 sr in version 2), within the range of possible lidar ratios for dust aerosols. However, recent statistical studies comparing CALIOP aerosol optical depth with other instruments reveal that CALIOP is generally biased low (Breon et al., 2011; Kittaka et al., 2011; Redemann et al., 2012), and especially in the case of dust aerosols (Schuster et al., 2012). The dust occurrence frequency (DOF) used here is reported with vertical resolution of 100 m and horizontal resolution of 1° and it is given by the equation:

$$\mathrm{DOF}(x,y,z) = \frac{\text{number of layers}(x,y,z)}{\text{total number of layers in the bin}(x,y)} \quad (1)$$

Figure 2 shows the number of dust layers (N) detected by CALIPSO at every bin for the four seasons. It can be observed the spatial distribution of SAL (where N greater

ACPD
13, 4727–4784, 2013

than about 500) and its northward shift between winter and summer. A similar seasonal spatial distribution of dust above Atlantic has been provided by MODIS dust optical depth (Ben-Ami et al., 2012, see their Fig. 1).

2.2 Additional data sets

For the same period, the MODIS/AQUA aerosol optical depth (AOD) at 550 nm is used (level 3, collection 5.1), which has a spatio-temporal resolution of 1° and 1 month. The aerosol characteristics from MODIS are derived over the land and oceans separately, using independent algorithms, while a third algorithm is used above bright surfaces, like deserts (Remer et al., 2005). Comparison of MODIS AOD retrievals with collocated AERONET measurements confirm that one standard deviation of MODIS AOD falls within the initial predicted uncertainty of $\Delta\tau = \pm 0.03 \pm 0.05\tau$ over ocean and $\Delta\tau = \pm 0.05 \pm 0.15\tau$ over land, more than 60 % of the time over ocean and more than 72 % of the time over land (Remer et al., 2005, 2008). It should be noted that MODIS observations due to their almost global coverage of the earth on a daily basis, their availability from both TERRA and AQUA satellites and their good quality have been used extensively to study dust aerosols above the Atlantic Ocean (e.g. Kaufman et al., 2005; Wong and Dessler, 2005; Kalashnikova and Kahn, 2008; Peyridieu et al., 2010; Ben-Ami et al., 2012; Peyridieu et al., 2012). MODIS AOD is used here as an additional constraint to DOF from CALIPSO regarding the spatial distribution of the SAL. At the same time, AOD being a parameter independent of DOF, offers an external validation of DOF, meaning that maxima (minima) of DOF should collocate with AOD maxima (minima), respectively. In Fig. 2 the MODIS 0.25 AOD isolines are superimposed to the number of dust layers detected by CALIPSO. As both parameters are column integrated, they can be directly compared. It can be seen that the areas with significant number of dust layers are mostly included in the 0.25 AOD isolines. This indicates that MODIS and CALIPSO are generally in agreement regarding the spatial occurrence of the SAL. However, some differences exist in winter and spring close to Africa south of the equator, in summer above middle Atlantic north of 20° N and in fall west of 30° W.

ACPD
13, 4727–4784, 2013

Nevertheless, these differences are minimized by plotting the MODIS 0.2 AOD isolines, especially in winter and spring, while in fall the differences persist west of 40° W (not shown). The discrepancies between CALIPSO number of dust layers and MODIS AOD in summer and fall will be further discussed in the next section. In any case it should be kept in mind when comparing the two quantities that a big number of dust layers does not necessarily mean that the layers are optically thick, especially far away from the Sahara or near the boundaries of SAL.

Wind strongly influences dust emission and transport (e.g. Maher et al., 2010). In order to examine the impact that may have the wind on SAL during its transport, wind data from ERA-Interim are used for the 5 yr of the study. ERA-Interim is the latest global atmospheric reanalysis produced by the ECMWF (Dee et al., 2011). The data are provided at a spectral T255 horizontal resolution, which corresponds to approximately 79 km spacing on a reduced Gaussian grid and at 37 pressure levels (from 1000 to 1 hPa). Here, the monthly means of daily means are used, as they are representative for the entire month. Then, the monthly means are averaged to seasonal means in order to be conformal with our CALIPSO dataset.

3 SAL seasonal vertical distribution

Figures 3 and 4 present the seasonal vertical distribution of the SAL above the Atlantic Ocean as depicted from CALIPSO measurements of dust aerosols. For each season, 5 latitude (x-axis)–altitude (y-axis) cross sections of DOF are shown with the latitude ranging from 10° S to 40° N, from the west coast of North Africa (10° W, bottom) to the east coast of South America and the east side of Caribbean Sea (50° W, top) with a step of 10°. Although, our database is available at a resolution of 1°, each cross section presents the meridional average of ±1° around the central longitude in order to increase the number of available data and to reduce the noise. The continuous bold colour line at the top of each cross section shows the MODIS AOD at 550 nm with the same colorscale as DOF, while below it the cyan line marks the ocean. Note that

ACPD
13, 4727–4784, 2013

the MODIS AOD at 10° W is not available from the standard algorithm above Sahara. White areas denote either very low DOF (< 0.05) or statistically insignificant number of dust layers (< 480 for the ±1° average). It can be seen in Figs. 3 and 4 that dust aerosols above tropical Atlantic are not found in general above the altitude level of 6.5 km (DOF < 0.05 above it) all year round. Also, an obvious seasonal cycle can be noticed, with the SAL being in contact with the surface, confined in a thin layer during winter, and more elevated, occupying a thicker layer during summer.

For completeness and in order to provide the spatial extension of the SAL as seen from CALIPSO, the DOF at six vertical levels from CALIPSO for the four seasons can be found in the Appendix (Figs. A1–A4). The six levels are: 1 km (left-bottom), 2 km (left-middle), 3 km (left-top), 3.5 km (right-bottom), 4.2 km (right-middle) and 4.8 km (right-top). These levels have been chosen in order to offer a good vertical description of the SAL and to match the existing pressure levels of the ECMWF wind data (at 900 hPa, 800 hPa, 700 hPa, 650 hPa, 600 hPa and 550 hPa), that will be used in the next section. Also, at every level the wind direction from ECMWF at this pressure is denoted by the black vectors, while the wind speed is given by the magenta isolines with step of $3\,m\,s^{-1}$. It must be mentioned that for these figures no averaging or smoothing has been applied to CALIPSO results.

The SAL is located by using the thresholds for DOF of 0.35 and for AOD of 0.2–0.25. The DOF being a relative magnitude is held constant for the whole region of interest, while as the AOD is an absolute magnitude its decrease with westward transport (e.g. Kalashnikova and Kahn, 2008) has been taken into account by applying a threshold of 0.25 close to Africa and 0.2 close to America. These thresholds are arbitrary, but they have been chosen by taking into account that away from Sahara and the main part of the SAL the DOF can take values up to 0.3 and the AOD up to 0.2. For comparison, the Maritime Aerosol Network (MAN) for the Atlantic indicated that 75 % of the data has AOD at 500 nm less than 0.2 (Smirnov et al., 2011, see also their Fig. 3a).

ACPD
13, 4727–4784, 2013

3.1 Winter (DJF)

During winter (Fig. 3-left), SAL is found between 5° S–15° N off West Africa (taking DOF > 0.35), while close to the coast of South America is observed between 5° S–10° N in accordance with MODIS AOD shown at the top of each cross section (taking AOD > 0.25) and with the results of Huang et al. (2010). The dust aerosols detected close to Africa (10° W to 30° W) north of 15° N and below 1.5 km are not part of the SAL, as it will be demonstrated by its seasonal evolution below and the wind fields in the next section. Vertically, SAL is observed between the surface and 3 km close to Africa, while by arriving at South America its top goes down to about 2 km. The SAL signature can be observed till 60° W (Figs. 2 and A1) with the top at the same level. Close to Africa (20° W), the maximum DOF is 0.6, found at 2 km collocated with the AOD maximum in the interval 5–10° N. Above South America (50° W), the maximum DOF (> 0.5) is located at 0.5 km near the equator.

South of 10° N, the biomass burning aerosols emitted during this period of the year are mixed with desert dust (Haywood et al., 2008). The important number of dust layers seen in Fig. 2 south of 5° N, is mostly due to the inclusion of the polluted dust class in the analysis, even if this inclusion does not impact the results. In fact, taking into account only the desert dust class of CALIPSO and not the combination of desert dust and polluted dust does not change the vertical distribution of Fig. 3-left (not shown). Thus, the inclusion of polluted dust class in the analysis does not modify the results for this region during winter. This can be explained by the fact that CALIPSO classifies the aerosol layers with relatively high estimated particulate depolarization ratio (> 0.2) as desert dust (Omar et al., 2009), which can comprise also dust and smoke mixtures. Indeed, lidar measurements above Cape Verde observed aerosol mixtures of biomass burning and desert dust having wavelength independent depolarization ratios between 0.12–0.23 (Gross et al., 2011). At 40° W, over South America it can be noticed that DOF takes relatively high values (> 0.5) from the surface up to 2 km. However, as they are observed south of 5° S are not part of the SAL (also notice that MODIS AOD is lower

ACPD
13, 4727–4784, 2013

than 0.05). The elevated DOF values could be related to the lower number of detected dust layers above South America (< 300) than over the nearby ocean (Fig. 2). It should be mentioned that the majority of dust layers detected over South America south of the equator from CALIPSO is polluted dust (not shown). Although, the contamination from local biomass burning aerosols can not totally excluded, the fire activity to the north and east of the Amazon Basin peaks in fall (van der Werf et al., 2003; Giglio et al., 2006), meaning that the majority of these layers are transported from Africa.

Near the African coast, measurements from recent campaigns during winter indicated a two-layer aerosol structure with desert dust up to 1.5–2 km and mixed dust/smoke aerosols above, reaching an altitude of 5 km (Johnson et al., 2008; McConnell et al., 2008; Tesche et al., 2011). Other studies, based on CALIPSO data, reported dust top height at about 3 km near the African coast (10° W–20° W) (Ben-Ami et al., 2009; Huang et al., 2010), in accordance with our results. As mentioned previously, this difference between CALIPSO and the field studies can be explained by the use of different ways (and instruments) to characterize a layer as desert dust and separate it from other aerosol types. While, it should be noted that mineral dust is also found even in aged elevated biomass burning layers over western Africa (at least north of 8° N), accounting for 72 % of the estimated aerosol mass (Formenti et al., 2008). Over the Atlantic a shipborne campaign found dust maximum height just above 2 km around 40° W (Voss et al., 2001), in agreement with Fig. 3-left. Further away, above South America, two studies reported Saharan dust below about 3 km, mostly well mixed with smoke (Ben-Ami et al., 2010; Baars et al., 2011). The Saharan dust aerosols fertilize the Amazon Basin during winter, which is very important for the maintenance of its nutrition balance (Kaufman et al., 2005; Koren et al., 2006), while they act as ice nuclei, thereby influencing precipitation and radiation budget over the Amazon sensitive ecosystem (Prenni et al., 2009). Although, Ben-Ami et al. (2010) have presented a case study of this transport, here a more general and completed picture is given using climatological data. However, especially above the Amazon there is still need of independent studies to further validate our results.

ACPD
13, 4727–4784, 2013

3.2 Spring (MAM)

Figure 3-right displays the results for spring. It can be observed that SAL moves 5° northwards both off West Africa (0–20° N) and off South America (0–15° N), although, the number of dust layers is reduced south of 5° N (Fig. 2). CALIPSO results are in accordance with MODIS observations close to Africa, while off South America although DOF values do not seem to decrease significantly north of 15° N, the number of dust layers is reduced to less than 500 (Fig. 2). Also, north of 20° N, dust layers can be observed scattered over the entire north Atlantic in contrast to the other seasons (Fig. 2), although their number is less than 300. These can be either dust mixed with anthropogenic pollution from North America or desert dust transported from Asia (e.g. Uno et al., 2009). Over eastern Atlantic, SAL occurs in the altitude range 1–4 km for its northern part (10–20° N) and between the surface and 3 km for its southern part (0–10° N). The higher altitude range at the north part of SAL (Fig. 3-right at 20° and 30° W) results from the influence of the trade winds, as shown in the next section. Its maximum altitude is reached at about 14° N, that is 5° north of the AOD maximum. The maximum DOF of 0.6 is found at 2–3 km, below the maximum altitude (14° N). Towards South America (and south Caribbean Sea for this season) SAL lies between the surface and 2–2.5 km, while the maximum DOF (∼ 0.55) is found around 10° N at 1.5 km. It can be detected till 70° W around 10° N (Figs. 2 and A2) at the same altitude range (not shown). In the same figures someone can observe dust layers beyond 70° W, however in northern South America spring is the season with the most fire activity (van der Werf et al., 2003; Giglio et al., 2006). Thus, results even after 60° W over land should be used and interpreted with caution, by keeping in mind that the majority of dust layers there (Fig. 2) belong to the polluted dust class (not shown). Like in winter, at 40° W over eastern South America (Fig. 3-right) relatively high DOF values can been seen below 2 km. Once again, this is not part of SAL, while also the number of dust layers there is limited (Fig. 2).

ACPD
13, 4727–4784, 2013

Leon et al. (2009) analyzing 3 yr of observations over a coastal site of Senegal, indicated that the dust layer top is located a little higher than what we found in this study, between 4 and 5 km during spring. On the other hand, over north-eastern South America, Formenti et al. (2001) found dust layers extended up to 700 hPa (~ 3 km). These last results are in agreement with Fig. 3-right. Despite the fact that the dust transport to northern South America peaks in spring (Prospero et al., 1981), there is lack of studies looking at the vertical distribution of dust in both sides of Atlantic during this season.

3.3 Summer (JJA)

Although the characteristic oval shape of SAL (Karyampudi et al., 1999; Liu et al., 2008b) starts to appear at its northern part during spring, it can be more clearly observed during summer (Fig. 4-left). In summer, SAL moves farther northward, occurring off West Africa between 5–30° N and between 10–25° N east of the Caribbean Sea, while it reaches Central America, south-eastern USA and the Gulf of Mexico (Figs. 2, 5 and A3). Also, SAL northern edge moves southwards till 50° W reaching 25° N, and then starts to turn northwards (Figs. 2, 4-left and 5), which is in accordance with the anticyclonic rotation of the SAL within the ridge region mentioned by Karyampudi et al. (1999). This is not obvious from the MODIS AOD 0.25 isoline in Fig. 2, but it can be observed from the AOD plotted at the top of each cross section of Figs. 4-left and 5. The comparison between winter and summer in Fig. 2 depicts clearly the seasonal latitudinal displacement of SAL, while it also shows the longer westward transport of dust during summer. Near Africa, SAL lies in the altitude range 1 to 5 km, with its maximum top at about 21° N when the AOD maximum is found at ~ 17° N, as in spring. This meridional shift between the maximum AOD and altitude observed in both seasons can be explained by the lower DOF, which indicates lower amount of dust aerosols, below the northern part of SAL in comparison to the southern one. A similar meridional shift was found between the maximum dust AOD and the temperature difference induced by dust outbreaks (Wilcox et al., 2010). At mid Atlantic (30–40° W) the base of SAL

ACPD
13, 4727–4784, 2013

increases to 1.5–2 km (more evident for the southern part of SAL), while the top decreases with westward transport, as for the other seasons. Around 50° W, a transition is seen with SAL presenting two parts, the south one (10–15° N) found between the surface and 3.5 km and the north one (15–25° N) between 1.5 and 4 km (Fig. 4-left). Again, this seems to be a result of the influence of the trade winds, examined in the next section. After 60° W, the SAL bottom appears to be in contact with the surface, while the top continues to decrease, reaching 2 km at 80° W (Fig. 5). The maximum DOF (> 0.5) is found about 3 km off West Africa (20° W) between 15° N and 25° N, decreasing to below 1 km at 80° W around 20° N. The maximum DOF appears to be collocated with the maximum warming of the SAL found at 2–3 km (Wang, 2009), especially for eastern Atlantic. Further west, the signature of the SAL is less clear as MODIS AOD is below 0.2, although CALIPSO see dust layers below 2 km.

The high values of DOF (> 0.6) south of the equator over South America, are not related at all with dust aerosols from Africa at it can been seen from the wind direction in Fig. A3. The dust layers seen there belong to the polluted dust class (not shown), while their origin could be attributed to the transport of biomass burning aerosols from fires in the Amazon Basin during late summer (Giglio et al., 2006). In the previous section have been noticed differences between CALIPSO number of dust layers and MODIS AOD north of 20° N, close to America (Fig. 2). This discrepancy is reduced by taking the 0.2 AOD isoline, which is found 2–3° northward of the 0.25 AOD isoline. The significant number of dust layers north of 23° N can be attributed to anticyclonic circulation observed close to 30° N and 50° W (Fig. A3). Indeed, the wind vectors in Fig. A3 indicate that a contamination of dust aerosols with North American pollution is unlikely. On the other hand, the dust aerosols north of 20° N can be entrapped in the anticyclonic circulation, and thus either deposited on mid Atlantic or dispersed during the transport, therefore decreasing their AOD. This can explain the discrepancy between MODIS AOD and CALIPSO number of dust layers.

In contrast with the other seasons there are more observations of SAL during summer and especially in the eastern Atlantic. Above Cape Verde, measurements of the

ACPD
13, 4727–4784, 2013

SAMUM-2b campaign indicate that the dust layer top is at 4.4 ± 0.7 km with a mean layer depth of 4.1 ± 0.7 km, above a 0.5–1.0 km deep maritime boundary layer (Tesche et al., 2011). Airborne measurements near Dakar above ocean registered dust up to 6 km (McConnell et al., 2008). Off West Africa, NAMMA airborne observations pointed out that the SAL generally extends up to 4 to 6.5 km, with a characteristic temperature inversion at its base at about 2 km (Ismail et al., 2010), in accordance with shipborne lidar measurements in the same region (Immler and Schrems, 2003). Also, SAGE II climatological data reveal one dust layer in the eastern north tropical Atlantic located between 2 and 6 km (Zhu et al., 2007). On the west side of Atlantic, results from the PRIDE campaign indicate that dust aerosols can reach an altitude of 5 km, presenting a highly variable vertical distribution and revealing the presence of dust in the marine boundary layer at Puerto Rico (Reid et al., 2002, 2003). Similar results were reported over Florida with case studies of dust layers from 1 to 4 km (DeMott et al., 2003) and from 1.7 to 5.5 km (Sassen et al., 2003). According to CALIPSO, in the area of Puerto Rico (20° N, 60–70° W), the dust layer is found mostly below 3 km, although some dust can be observed up to 4.5–5 km (DOF ∼ 0.1) (Fig. 5).

3.4 Fall (SON)

Finally, during fall (Fig. 4-right), SAL turns back southward, lying between 0–25° N off West Africa and between 5–20° N at 50° W, by taking into account also the MODIS AOD and the number of dust layers from CALIPSO. In the vertical, dust aerosols are found between the surface and 3 km close to Africa, while, east of the Caribbean Sea, the top decreases to 2 km. However, after 40° W, MODIS AOD is close to 0.1, a typical value for remote maritime regions (Smirnov et al., 2011), thus indicating the absence of significant dust load farther west. On the other hand, CALIPSO DOF does not present any obvious change, although the available number of dust layers is reduced (Fig. 2). This manifests the limits of the DOF, which does not permit a quantitative description of the dust load, and renders the position of the northern border of SAL above mid-Atlantic less accurate during this season. Also, there is not an obvious maximum of

ACPD
13, 4727–4784, 2013

DOF neither close to Africa nor close to Caribbean Sea. The high DOF values at 40° W above South America can rather be linked to fire activity which peaks in fall (van der Werf et al., 2003; Giglio et al., 2006), confirmed by the wind direction in Fig. A4. Leon et al. (2009) reported a layer between 1 and 2 km above a coastal site in Senegal, even if in their results there is significant interannual variability with aerosols from the surface up to 3–4 km during some years. It should be underlined the lack of studies during this season, in part due to less strong dust outbreaks (Ben-Ami et al., 2012).

3.5 Zonal evolution of the SAL characteristics

As, the spatial extension of the SAL and its limits are described previously, we focus now on its zonal evolution above the Atlantic. Figure 6 presents the vertical distribution of CALIPSO DOF at one longitude for each season at: 5° N for winter, 10° N for spring and 15° N for summer and fall. As SAL shifts latitudinally during the different seasons, the latitudes have been chosen in order to be representative of SAL central part during each season. Figure 6 is similar to Figs. 3 and 4, but now the horizontal axis is the longitude from 10° W to 80° W. Data after 60° W for winter and fall or after 70° W for spring have been removed because of the limited number of dust layers (Fig. 2).

It can be observed that the altitude decrease of SAL with westward transport is smooth for all seasons. Once, SAL leaves Africa is found in contact with the ocean surface during winter and fall. In contrast during spring its base is found at 1 km from 20° W to 40° W. This is also the case in summer, with the base located at 1.5 km between 15° W and 50° W, while from 20° W to 30° W the DOF is lower than 0.2. Figure 6 further corroborates the results seen in Figs. 3-right and 4-left for spring and summer, with lower DOF values below the SAL (especially its northern part) at eastern Atlantic. At the top of each cross section, it can be seen a decrease of MODIS AOD with westward transport, while the DOF values do not seem change significantly, although higher DOF values are found over Africa. This underlies the difference between the use of relative and absolute magnitudes in the description of the SAL evolution.

ACPD
13, 4727–4784, 2013

Figures 3, 4 and 6 indicate that the SAL is not characterized by a multilayer structure, but rather it can be described by a single layer (at least climatologically). This is in agreement with the climatology of SAGE II off West Africa during summer (Zhu et al., 2007) (a second dust layer below 1 km seen in their Fig. 7, can be explained by the transport of dust at lower levels during the rest of the year). On the other hand, Ben-Ami et al. (2009) using the first year of CALIPSO data noticed a two-layer structure of dust above Atlantic especially during summer, with the lower one attached or within the marine boundary layer. This is no longer found here. In Fig. 4-left south of 20° N, it can be observed that below 1.5 km there are indeed dust aerosols (DOF = 0.2–0.3), although below the SAL. The picture of the SAL as a single layer is also in agreement with the cases studies of Karyampudi et al. (1999); Liu et al. (2008b); Ben-Ami et al. (2010) and with the example of Fig. 1. Thus, the use of notions like mean altitude and mean geometrical thickness are adequate to describe it.

Figure 7 presents the mean altitude (a.s.l.) and geometrical thickness, averaged over 10° in latitude, for the four seasons between Africa (10° W) and America (90° W). The 10° zone is different among the four seasons in order to depict the central part of the SAL during its westward transport. Although, during spring and fall, there are few data after 70° W and 60° W, respectively, these have been removed because of the limited number of detected dust layers. The thin dotted lines are the linear fit in the interval 10–50° W for winter, 20–60° W for spring and fall and 30–80° W for summer. It is reminded that the results after 60° W in spring are less reliable due to the peak of fire activity in northern South America.

Figure 7 indicates that there is a clear distinction between winter and summer both for the altitude (left) and the geometrical thickness (right), with higher values during summer. The transition seasons of spring and fall show similar characteristics, with the values of altitude and geometrical thickness bounded by the respective values of winter and summer. Both mean altitude and geometrical thickness are decreasing from Africa to America, except altitude during summer, which stays approximately constant at 3 km up to 30° W and then decreases. The SAL mean altitude decreases with

ACPD
13, 4727–4784, 2013

westward transport by 13 m deg^{-1} in winter, 24 m deg^{-1} in spring and 23 m deg^{-1} in fall (with the mean altitude being 200 m higher during spring) and 28 m deg^{-1} in summer. Ben-Ami et al. (2009) used the first year of CALIPSO data and found that the top altitude decreases by 23 m deg^{-1} in winter (about twice than our results) and 27 m deg^{-1} in summer (similar with our results). The SAL mean geometrical thickness also regularly decreases, but with higher rates in winter than in summer (contrary to altitude), while spring and fall have similar rates. Between 10° W and 20° W, SAL geometrical thickness reduces sharply, due to transit from land to ocean, except during winter where the central part of SAL is mostly above ocean. The decrease rate is 25 m deg^{-1} in winter, 13 m deg^{-1} in spring, 9 m deg^{-1} in summer and 14 m deg^{-1} in fall. The decrease of SAL altitude and geometrical thickness with westward transport can be attributed to the descent of the dust aerosols by sedimentation and large scale subsidence, with wet removal modulating these processes (Colarco et al., 2003). On the other hand, the clear sky subsidence due to longwave radiative cooling, also depending on the water vapour content, is another factor contributing to the observed decrease (Huang et al., 2010).

Results of SAL mean altitude and its decrease with westward transport (Fig. 7) coupled to the mean wind speed (Figs. A1–A4) allow estimating the effective dry deposition velocity of dust particles. The mean altitude of SAL is between 1.5–2 km in winter, 1.5–2.5 km in spring and fall, and 1.5–3 km in summer (Fig. 7-left). These values correspond to pressure levels of about 700–800 hPa for summer and about 800 hPa for the other seasons. Figures A1–A4 indicate that the wind speed at these pressure levels is ∼ 8 m s^{-1} for summer (see also Fig. 9-left of the next section) and ∼ 6–7 m s^{-1} for the other seasons. By taking that 1 degree of longitude equals about 110 km near the equator, this means that 1 degree is covered in about 5 h for wind speed of 6 m s^{-1}. In the same time period, the SAL mean altitude decreases with the values mentioned in the previous paragraph. Thus, accounting for the average seasonal wind speed, the effective dry deposition velocity of dust particles is 0.07–0.08 cm s^{-1} in winter, 0.13–0.15 cm s^{-1} in spring and fall, and 0.2 cm s^{-1} in summer, which is about 3 times larger

ACPD
13, 4727–4784, 2013

than for winter. The term effective is used here because the velocities are based on SAL mean altitude decrease and the wind speed from ECMWF, which account for all the processes relevant to the deposition of dust particles, like gravitational settling, turbulent mixing, Brownian diffusion, particle inertia, particle drag (Noll and Aluko, 2006; Foret et al., 2006) and the atmospheric subsidence. It should be noted that according to PRIDE observations, Stokes settling is too strong and an upward velocity is needed to account for the changes in dust particle size distribution (Maring et al., 2003). Generally, dry deposition velocities for dust particles are estimated close to 1 $cm\,s^{-1}$ (Dulac et al., 1992), but our results lie within a plausible range. Prospero et al. (2010) reported dry deposition velocities in the range 0.23–0.89 $cm\,s^{-1}$ during summer, which are in accordance with our results given the large uncertainties. However, for winter months they found very large deposition velocities in the range 1.30–3.13 $cm\,s^{-1}$, which are values much higher than our results. In addition, their winter results are higher than the summer ones, which is in contrast with our findings. The discrepancies can be explained by the different approaches to estimate the dry deposition of dust particles, and by the fact that we are looking here to a more representative climatological dataset.

4 Impact of wind on SAL shape

Once the vertical distribution of the SAL has been established and validated against observations from other studies, the next step is to examine the impact that may have the wind field on the SAL shape. Figures 8 and 9 present the seasonal horizontal wind from the ERA-Interim data averaged over the same period as CALIPSO observations, at three pressure levels: 900 hPa (~ 1 km, bottom), 700 hPa (~ 3 km, middle) and 500 hPa (~ 5.5 km, top). Also, in order to facilitate the interpretation of the interaction between SAL and wind, the MODIS AOD isolines of 0.25 and 0.5 are plotted as indicative of the SAL location and dust load. To avoid any misinterpretation of the isolines above Sahara, it is reminded that MODIS (standard algorithm) does not provide results above deserts. As mentioned in the previous section, Figs. A1–A4 present the

ACPD
13, 4727–4784, 2013

CALIPSO DOF at six levels with the wind direction and speed from ECMWF, and they are supplementary to Figs. 8 and 9.

4.1 Winter

During winter, at low tropospheric levels (900 hPa), the wind flow is northeasterly above the equator bringing dust from Africa to South America (Fig. 8-left). However, away from the SAL, it can be observed that north of 25° N the wind direction changes from easterly to westerly, due to high pressure systems located over the Atlantic between 20–30° N most of the year (Christopher and Jones, 2010). At 700 hPa, the wind in the eastern tropical Atlantic is easterly up to 15° N and then shifts to westerly, with the shift arriving now southern than the respective at 900 hPa. This change in the wind direction with altitude is observed in Fig. 3-left at 20° W with the quasi absence of dust aerosols north of 15° N above 2 km (as already mentioned, this latitude coincides with the northern border of the SAL during winter). The southern swift of the wind direction change with altitude can be discerned more easily in Fig. A1. No dust aerosols are seen at 500 hPa in winter (see previous section). In agreement with these results, winter observations at Cape Verde indicate dust transport at low altitudes (below 1.5–3 km) by the trade winds Chiapello et al. (1995). Likewise, dust transport up to 2–3 km within the trade wind layer has been obtained from a regional model (Schepanski et al., 2009).

4.2 Spring

In spring (Fig. 8-right), off West Africa at 900 hPa, the wind direction is north-northeast bringing air masses from North Atlantic down to 10–15° N, thus mostly clean maritime air without dust aerosols, while farther south, down to equator, the flow brings air masses from Sahara. This observation can explain the decrease of DOF at low levels seen in Fig. 3-right (10–20° N, 20–40° W) and the DOF local minimum in the same region (DOF < 0.35) observed in Fig. A2 at 900 hPa. Farther west, dust aerosols are found in contact with the surface due to the decrease of the SAL altitude with

ACPD
13, 4727–4784, 2013

transport, though the relatively high speed ($> 7\,m\,s^{-1}$) of dust-free air masses in mid Atlantic (Fig. 8-right) counters the subsidence at 40° W between 10–15° N (Fig. 3-right). At 700 hPa, there is a change of wind direction from easterly to westerly at about 20° N, which does not permit the development of SAL farther northwards at this altitude, thus confirming the horizontal extension of the SAL up to 20° N seen in the previous section. Although there are not dust aerosols at 500 hPa during spring, it should be noted that, at this level, the change of wind direction happens south of 10° N. This southern shift with altitude of the direction change can explain the ellipsoid shape on the north part of the SAL seen in Fig. 3-right.

4.3 Summer

At 900 hPa during summer, the trade winds import clean air from both hemispheres below the SAL at least up to 40° W (Figs. 9-left and A3). Also, their high speed ($> 7\,m\,s^{-1}$) prevents the subsidence of dust aerosols up to 40° W for the southern part and up to 50° W for the northern part, in accordance with Fig. 4-left. At 700 hPa, the flow is easterly up to about 30° N, transporting directly the SAL to the Caribbean Sea, with strong wind ($> 7\,m\,s^{-1}$) between 10° N and 20° N, where the maximum AOD of the SAL is seen (Fig. 4-left). After 60° W, the flow turns to southeasterly, thus bringing dust aerosols to Southeast USA and Gulf of Mexico. Above at 500 hPa, the flow remains easterly, but up to ~ 25° N this time, while the wind magnitude is significant up to 40° W, meaning a more efficient westward transport of dust aerosols at this altitude till this longitude. As in spring, the oval shape seen in the north edge of the SAL (Fig. 4-left) can be explained by the southern shift of wind direction change with altitude (more easily to depict in Fig. A3). The role of relatively clean northeasterly trade winds that erode the low-lying dust aerosols along the African coast during the westward transport has been also noticed by previous studies (Karyampudi et al., 1999; Colarco et al., 2003). The wet removal can be also a contributing factor to dust erosion at low levels, while some of the low-level dust may persist all the way across the ocean (Colarco

ACPD
13, 4727–4784, 2013

et al., 2003), as it can be observed in Fig. 4-left (below SAL, DOF values 0.1–0.2). A model study showed as well that in summer dust is transported above the trade winds inversion (Schepanski et al., 2009).

4.4 Fall

During fall, at 900 hPa the wind is mostly easterly, but being southeasterly below ~ 5° N and northeasterly around 20° N (Fig. 9-right). Indeed, in Fig. 4-right at 20° W and about 25° N, there is a minimum of DOF, in relation with the transport of dust-free air masses from the north (see also Fig. A4). At 700 hPa, the flow is easterly up to 20–25° N and then changes direction to westerly. Again, north of 20–25° N, there are no dust aerosols (Fig. 4-right).

4.5 The role of Intertropical Convergence Zone (ITCZ)

The south border of the SAL is closely connected all year round to the position of the ITCZ (Marticorena et al., 2011; Ben-Ami et al., 2012). Based on climatological data above the Atlantic, the ITCZ stays north of the equator almost all time of year and its position is about 3° N during winter and spring (may be southern), 10° N during summer and 8° N during autumn (Waliser and Gautier, 1993; Hu et al., 2007; Zagar et al., 2011). The same studies found the ITCZ position over South America around 10° S during winter, although large variations make it difficult to localize it precisely and 3° S during spring. The approximate ITCZ position can be seen at 900 hPa on Figs. 8 and 9, where the meridional wind is zero (Zagar et al., 2011, in their study the meridional wind averaged over 10 pressure levels of ERA Interim data below 900 hPa have been used). For the 5-yr period examined here, during winter the ITCZ seems to be slightly north of the equator (5° N close to Africa and 2° N close to South America) above the Atlantic, going down to at least 10° S over South America. During spring, it seems to be over the equator both above the Atlantic and South America, while during summer and fall over the Atlantic is at 10° N and 8° N, respectively. From the results of

ACPD
13, 4727–4784, 2013

the previous section and the approximate position of the ITCZ, it can be observed that above western Atlantic or South America, the SAL either is bounded by the ITCZ in the south (spring, summer and fall) or it never reaches it (winter) (Figs. 8 and 9-bottom). However, over eastern Atlantic the restriction of the SAL in the south by ITCZ can be clearly seen only during spring, while during winter and summer both CALIPSO and MODIS indicate the existence of dust aerosols, even south of ITCZ. During summer and fall, the number of dust layers from CALIPSO is significantly reduced south of ITCZ (located at 10° N and 8° N, respectively) in comparison to northern latitudes (Fig. 2). In addition only a small part of SAL is found south of 10° N at about 3 km during summer (Fig. 4-left). This indicates that near Africa, ITCZ is not a rigorous south border of SAL during these two seasons, but it rather prevents a large number of dust layers to run through it. On the other hand, in winter, there is not a simple explanation to the fact that SAL penetrates into ITCZ (one possible reason may be the weaker intensity of ITCZ over east Atlantic during winter (Waliser and Gautier, 1993, see their Fig. 1)).

4.6 African Easterly Jet and SAL

An important feature that can be noticed in Figs. 8 and 9 at 700 hPa (middle) is the collocation of SAL AOD maximum with a local maximum of the wind speed over the coast of West Africa for all seasons. This wind maximum, actually the African Easterly Jet (AEJ) (Wu et al., 2009; Lafore et al., 2011), is climatologically located at about 2° N, 700 hPa in winter and at 14° N, 600 hPa in summer (Afiesimama, 2007), few degrees southward than seen in Figs. 8 and 9. The coincidence between AEJ and SAL in the vertical mostly happens at the upper levels of the SAL, as the AEJ is placed above 2 km in winter, going to above 3 km in summer. Thus, the transport of dust aerosols in the upper levels of the SAL is realised within the AEJ close to Africa, which promotes the differential advection between the upper and lower parts of SAL. Karyampudi et al. (1999) mentioned that the SAL is transported westward by the AEJ (in their study named middle level easterly jet), located near the southern edge of the SAL. However, firstly the AEJ is found mostly near western Africa in contrast to SAL that reaches

ACPD
13, 4727–4784, 2013

America and secondly SAL presents higher extension than AEJ, spatially and vertically. These indicate that SAL is not transported by AEJ, but only a part of SAL interacts with AEJ. On the other hand, Tompkins et al. (2005) have shown that a better description of aerosols especially over Sahara in the ECMWF model significantly improved the forecast of AEJ structure and strength, via the direct radiative forcing. In addition, the AEJ is accelerated by approximately 4 $m s^{-1}$ and is moved northward by 4–5 degrees during dust outbreaks compared to low dust conditions (Wilcox et al., 2010). Thus, a strong interconnection between SAL and AEJ exists that should be further studied. A first step to this end has been realised during the AMMA campaign, where the impact of SAL on African Easterly Waves (which develop though barotropic and baroclinic energy conversions as they move along the AEJ) has been examined (Zipser et al., 2009; Ismail et al., 2010; Lafore et al., 2011).

5 Summary and conclusions

In this study, the vertical distribution of the Saharan Air Layer (SAL) is presented based on the detection of dust aerosols from CALIPSO above the Atlantic. 5 yr CALIPSO observations of desert dust and polluted dust layers are used to depict the seasonal vertical distribution of SAL with 1° horizontal resolution. These results offer a better description of the SAL, not accessible up to now, at least vertically. The desert dust and polluted dust classes have been merged in order to take into account the mixing of desert dust with other aerosol types (pollution, biomass burning, maritime), the ageing of desert dust during its long range transport to America and the possible misclassification of desert dust as polluted dust by the CALIPSO algorithms. Also, the possible overlap/overwrite of the layers has been taken into account and corrected. Use is made of dust occurrence frequency (DOF) in order to avoid the assumption about the lidar ratio, while the MODIS aerosol optical depth at 550 nm is also used as an additional and independent parameter to validate the spatial distribution of the SAL. The quality of our results is conditioned by the good quality of CALIOP signal and the sound performance

ACPD
13, 4727–4784, 2013

of CALIPSO algorithms to detect the boundaries of aerosol or cloud layers, to discriminate aerosols from clouds and to recognize dust aerosols from other classes due to depolarization ratio. It must be noted that the majority of previous studies (e.g. Karyampudi et al., 1999; Dunion and Velden, 2004; Zhu et al., 2007; Zipser et al., 2009; Braun, 2010; Nalli et al., 2011; Davidi et al., 2012) examined the SAL characteristics mainly during late spring to early fall when the dust load is more significant and the hurricanes and tropical cyclones activity peaks. Albeit, it has been shown that SAL exists all year round at least in relation to dust aerosols examined here.

The CALIPSO data indicates that SAL presents a clear seasonal cycle and appears northern in latitude and higher in altitude during summer than during winter. This seasonality is in accordance with the results of Prospero et al. (2012) (see their Fig. 3). Spatially, at 20° W, it is found between 5° S–15° N in winter going at 5–30° N in summer. Towards east Caribbean Sea (50° W), SAL is observed in the interval 5° S–10° N in winter and at 10–25° N in summer, although it can reach the longitudes of 60° W during winter and 90° W in summer. During, the transitory seasons of spring and fall, SAL is found between the position of winter and summer not only spatially, but also vertically. In winter, SAL occurs in the altitude range 0 to 3 km at 20° W, going to 0–2 km eastern of South America (50° W). During summer, SAL is found more elevated close to Africa (20° W) at 1 to 5 km going down to 0–2 km in the Gulf of Mexico (80–90° W). These results are generally in accordance with previous studies, although, the majority of these studies only deal with a limited number of cases, mainly in summer and close to West Africa.

The vertical distribution of SAL does not generally show a multi-layer structure, but rather only one dust layer, which justifies the use of notions as mean altitude and mean geometrical thickness. During winter the mean altitude decreases with westward transport by 13 m deg^{-1} and the mean geometrical thickness by 25 m deg^{-1}, while in summer the mean altitude decreases after 30° W by 28 m deg^{-1} and the mean geometrical thickness by 9 m deg^{-1}. Thus, the decrease tendency is inverted between the altitude and geometrical thickness during the two opposite seasons, while the two

ACPD
13, 4727–4784, 2013

transition seasons present similar characteristics. The abovementioned results with the wind speed from ECMWF permit to estimate the effective dry deposition velocity of dust particles. This is 0.07–0.08 $cm\,s^{-1}$ in winter, 0.13–0.15 $cm\,s^{-1}$ in spring and fall, and 0.2 $cm\,s^{-1}$ in summer.

We have shown that the wind field not only determines the transport of SAL, but also modulates its shape. During winter the trade winds transport SAL towards South America, while in spring and summer they scavenge dust aerosols below SAL by bringing maritime air masses from North Atlantic up to about 50° W, in accordance with previous studies. The trade winds from the Southern Hemisphere scavenge less efficiently the low levels of SAL southern part, but its structure can be still clearly observed. On the other hand, the North Atlantic westerlies, with their southern border occurring between 15° and 30° N (depending on the season, the longitude and the altitude), prevent the SAL to develop further northward. In addition, their southward shift with altitude gives to SAL its characteristic oval shape in its northern part, as shown here for the first time to the best of our knowledge. Concerning the southern part of the SAL, the ITCZ is the central feature that determines its southern border. However, above the eastern tropical Atlantic some dust layers can be seen in or south of the ITCZ, indicating that ITCZ does not inhibit the penetration of dust aerosols, but rather reduces it significantly. Also, it was observed that the AEJ collocates with the maximum dust load, a fact that may induce the development of differential advection within the SAL, especially during summer.

These results should be helpful to examine how well models reproduce the SAL vertical distribution on a seasonal scale or could be used as input data to models describing the vertical distribution of dust aerosols above the Atlantic (e.g. Koffi et al., 2012). Also, they can be used as a priori information (vertical distribution of dust aerosols) into satellite algorithms, which analyse data from instruments either in the UV spectrum, like TOMS or OMI, or in the IR spectrum, like AIRS or IASI, in order to improve the quality of their geophysical retrievals, as these instruments are sensitive to the vertical distribution. Further, as there are growing efforts in order to obtain the height of

ACPD
13, 4727–4784, 2013

aerosols plumes from passive satellite instruments (Kahn et al., 2007; Joseph et al., 2008; Kokhanovsky and Rozanov, 2010; Peyridieu et al., 2010, 2012), these results comprise a validation dataset.

Finally, there is a need of systematic measurements of the SAL vertical distribution not only at both sides of Atlantic but also over it, in order to further validate the CALIPSO results presented here. A step forward has been achieved with the AEROSE shipborne campaigns (Nalli et al., 2005, 2011), which observed the SAL vertical distribution using mainly radiosondes and sunphotometer data at the ship level. However, because dry air outbreaks from Africa into the tropical Atlantic are not always related to African dust outbreaks (Zhang and Pennington, 2004) and also due to connection of SAL with wind (and AEJ), future campaigns or long-term measurement sites should combine vertical measurements of dust aerosols, temperature, humidity and wind reaching at least up to 7 km, in order not to miss the upper parts of SAL, according to the results presented here. The combination of all these parameters is important if we want to understand in depth the impacts of SAL on the environment over Atlantic and the adjacent continents.

Appendix A

The Figs. A1–A4 are presented here as additional material, in order to give a more complete picture of the SAL by exploiting the main advantage of CALIOP, which is its fine vertical resolution. Also, they provide the spatial extension of the SAL as seen from CALIPSO. For every season, the DOF is depicted at six vertical levels, which correspond to pressure levels of ERA-Interim data at: 900 hPa (~ 1 km), 800 hPa (~ 2 km), 700 hPa (~ 3 km), 650 hPa (~ 3.5 km), 600 hPa (~ 4.2 km) and 550 hPa (~ 4.8 km). At every level the wind direction from ECMWF at this pressure is denoted by the black vectors, while the wind speed is given by the magenta isolines with step of 3 $m\,s^{-1}$.

ACPD
13, 4727–4784, 2013

Acknowledgements. CALIPSO NASA and CNES scientific teams and MODIS scientific team are gratefully acknowledged for providing high quality satellite data. We thank NASA/LaRC and ICARE Data and Services Center (http://www.icare.univ-lille1.fr) for providing us with CALIPSO data. MODIS data were obtained through NASA's Giovanni, developed and maintained by the NASA GES DISC. S. Peyridieu is acknowledged for assistance regarding acquisition of CALIPSO data. This work has been supported in part by the European Community under the contract FP7/MACC II project, Grant Agreement no. 283576.

The publication of this article is financed by CNRS-INSU.

References

Adams, A. M., Prospero, J. M., and Zhang, C.: CALIPSO-derived three-dimensional structure of aerosol over the Atlantic Basin and adjacent continents, J. Climate, 25, 6862–6879, doi:10.1175/JCLI-D-11-00672.1, 2012. 4732

Afiesimama, E. A.: Annual cycle of the mid-tropospheric easterly jet over West Africa, Theor. Appl. Climatol., 90, 103–111, doi:10.1007/s00704-006-0284-y, 2007. 4752

Alpert, P., Kaufman, Y. J., Shay-El, Y., Tanre, D., da Silva, A., Schubert, S., and Joseph, J.: Quantification of dust-forced heating of the lower troposphere, Nature, 395, 367–370, 1998. 4729

Andreae, M. O. and Crutzen, P. J.: Atmospheric aerosols: biogeochemical sources and role in atmospheric chemistry, Science, 276, 1052–1058, 1997. 4734

Ansmann, A., Baars, H., Tesche, M., Muller, D., Althausen, D., Engelmann, R., Pauliquevis, T., and Artaxo, P.: Dust and smoke transport from Africa to South America: Lidar profiling over Cape Verde and the Amazon rainforest, Geophys. Res. Lett., 36, L11802, doi:10.1029/2009GL037923, 2009. 4731, 4734

ACPD
13, 4727–4784, 2013

Baars, H., Ansmann, A., Althausen, D., Engelmann, R., Artaxo, P., Pauliquevis, T., and Souza, R.: Further evidence for significant smoke transport from Africa to Amazonia, Geophys. Res. Lett., 38, L20802, doi:10.1029/2011GL049200, 2011. 4740

Balis, D. S., Amiridis, V., Nickovic, S., Papayannis, A., and Zerefos, C.: Optical properties of Saharan dust layers as detected by a Raman lidar at Thessaloniki, Greece, Geophys. Res. Lett., 31, L13104, doi:10.1029/2004GL019881, 2004. 4735

Ben-Ami, Y., Koren, I., and Altaratz, O.: Patterns of North African dust transport over the Atlantic: winter vs. summer, based on CALIPSO first year data, Atmos. Chem. Phys., 9, 7867–7875, doi:10.5194/acp-9-7867-2009, 2009. 4732, 4740, 4746, 4747

Ben-Ami, Y., Koren, I., Rudich, Y., Artaxo, P., Martin, S. T., and Andreae, M. O.: Transport of North African dust from the Bodélé depression to the Amazon Basin: a case study, Atmos. Chem. Phys., 10, 7533–7544, doi:10.5194/acp-10-7533-2010, 2010. 4732, 4740, 4746

Ben-Ami, Y., Koren, I., Altaratz, O., Kostinski, A., and Lehahn, Y.: Discernible rhythm in the spatio/temporal distributions of transatlantic dust, Atmos. Chem. Phys., 12, 2253–2262, doi:10.5194/acp-12-2253-2012, 2012. 4736, 4745, 4751

Braun, S. A.: Reevaluating the role of the Saharan Air Layer in Atlantic tropical cyclogenesis and evolution, Mon. Weather Rev., 138, 2007–2037, doi:10.1175/2009MWR3135.1, 2010. 4730, 4732, 4754

Breon, F.-M., Vermeulen, A., and Descloitres, J.: An evaluation of satellite aerosol products against sunphotometer measurements, Remote Sens. Environ., 115, 3102–3111, doi:10.1016/j.rse.2011.06.017, 2011. 4735

Bristow, C. S., Hudson-Edwards, K. A., and Chappell, A.: Fertilizing the Amazon and equatorial Atlantic with West African dust, Geophys. Res. Lett., 37, L14807, doi:10.1029/2010GL043486, 2010. 4731

Cattrall, C., Reagan, J., Thome, K., and Dubovik, O.: Variability of aerosol and spectral lidar and backscatter and extinction ratios of key aerosol types derived from selected Aerosol Robotic Network locations, J. Geophys. Res., 110, D10S11, doi:10.1029/2004JD005124, 2005. 4735

Chen, S.-H., Wang, S.-H., and Waylonis, M.: Modification of Saharan air layer and environmental shear over the eastern Atlantic Ocean by dust-radiation effects, J. Geophys. Res., 115, D21202, doi:10.1029/2010JD014158, 2010. 4730

Chiapello, I., Bergametti, G., Gomes, L., Chatenet, B., Dulac, F., Pimenta, J., and Santos Suares, E.: An additional low layer transport of Sahelian and Saharan

ACPD
13, 4727–4784, 2013

dust over the North-Eastern Tropical Atlantic, Geophys. Res. Lett., 22, 3191–3194, doi:10.1029/95GL03313, 1995. 4731, 4749

Christopher, S. A. and Jones, T. A.: Satellite and surface-based remote sensing of Saharan dust aerosols, Remote Sens. Environ., 114, 1002–1007, doi:10.1016/j.rse.2009.12.007, 2010. 4749

Colarco, P. R., Toon, O. B., Reid, J. S., Livingston, J. M., Russell, P. B., Redemann, J., Schmid, B., Maring, H. B., Savoie, D., Welton, E. J., Campbell, J. R., Holben, B. N., and Levy, R.: Saharan dust transport to the Caribbean during PRIDE: 2. Transport, vertical profiles, and deposition in simulations of in situ and remote sensing observations, J. Geophys. Res., 108, 8590, doi:10.1029/2002JD002659, 2003. 4747, 4750

Davidi, A., Kostinski, A. B., Koren, I., and Lehahn, Y.: Observational bounds on atmospheric heating by aerosol absorption: radiative signature of transatlantic dust, Geophys. Res. Lett., 39, L04803, doi:10.1029/2011GL050358, 2012. 4729, 4754

de Reus, M., Fischer, H., Sander, R., Gros, V., Kormann, R., Salisbury, G., Van Dingenen, R., Williams, J., Zöllner, M., and Lelieveld, J.: Observations and model calculations of trace gas scavenging in a dense Saharan dust plume during MINATROC, Atmos. Chem. Phys., 5, 1787–1803, doi:10.5194/acp-5-1787-2005, 2005. 4730

Dee, D. P., Uppala, S. M., Simmons, A. J., Berrisford, P., Poli, P., Kobayashi, S., Andrae, U., Balmaseda, M. A., Balsamo, G., Bauer, P., Bechtold, P., Beljaars, A. C. M., van de Berg, L., Bidlot, J., Bormann, N., Delsol, C., Dragani, R., Fuentes, M., Geer, A. J., Haimberger, L., Healy, S. B., Hersbach, H., Holm, E. V., Isaksen, L., Kallberg, P., Kohler, M., Matricardi, M., McNally, A. P., Monge-Sanz, B. M., Morcrette, J.-J., Park, B.-K., Peubey, C., de Rosnay, P., Tavolato, C., Thepaut, J.-N., and Vitart, F.: The ERA-Interim reanalysis: configuration and performance of the data assimilation system, Q. J. Roy. Meteorol. Soc., 137, 553–597, doi:10.1002/qj.828, 2011. 4737

DeMott, P. J., Sassen, K., Poellot, M. R., Baumgardner, D., Rogers, D. C., Brooks, S. D., Prenni, A. J., and Kreidenweis, S. M.: African dust aerosols as atmospheric ice nuclei, Geophys. Res. Lett., 30, 1732, doi:10.1029/2003GL017410, 2003. 4730, 4744

Doherty, O. M., Riemer, N., and Hameed, S.: Saharan mineral dust transport into the Caribbean: observed atmospheric controls and trends, J. Geophys. Res., 113, doi:10.1029/2007JD009171, 2008. 4731

ACPD
13, 4727–4784, 2013

Dulac, F., Tanre, D., Bergametti, G., Buat-Menard, P., Desbois, M., and Sutton, D.: Assessment of the African airborne dust mass over the western Mediterranean Sea using Meteosat data, J. Geophys. Res., 97, 2489–2506, doi:10.1029/91JD02427, 1992. 4748

Dunion, J. P. and Marron, C. S.: A reexamination of the Jordan mean tropical sounding based on awareness of the Saharan Air Layer: results from 2002, J. Climate, 21, 5242–5253, doi:10.1175/2008JCLI1868.1, 2008. 4729

Dunion, J. P. and Velden, C. S.: The impact of the Saharan Air Layer on Atlantic tropical cyclone activity, B. Am. Meteorol. Soc., 85, 353–365, doi:10.1175/BAMS-85-3-353, 2004. 4730, 4754

Evan, A. T., Dunion, J., Foley, J. A., Heidinger, A. K., and Velden, C. S.: New evidence for a relationship between Atlantic tropical cyclone activity and African dust outbreaks, Geophys. Res. Lett., 33, L19813, doi:10.1029/2006GL026408, 2006. 4730

Evan, A. T., Vimont, D. J., Heidinger, A. K., Kossin, J. P., and Bennartz, R.: The role of aerosols in the evolution of tropical North Atlantic Ocean temperature anomalies, Science, 324, 778–781, doi:10.1126/science.1167404, 2009. 4730

Evan, A. T., Foltz, G. R., Zhang, D., and Vimont, D. J.: Influence of African dust on ocean-atmosphere variability in the tropical Atlantic, Nat. Geosci., 4, 762–765, doi:10.1038/NGEO1276, 2011. 4730

Foret, G., Bergametti, G., Dulac, F., and Menut, L.: An optimized particle size bin scheme for modeling mineral dust aerosol, J. Geophys. Res., 111, D17310, doi:10.1029/2005JD006797, 2006. 4748

Formenti, P., Andreae, M. O., Lange, L., Roberts, G., Cafmeyer, J., Rajta, I., Maenhaut, W., Holben, B. N., Artaxo, P., and Lelieveld, J.: Saharan dust in Brazil and Suriname during the Large-Scale Biosphere-Atmosphere Experiment in Amazonia (LBA)-Cooperative LBA Regional Experiment (CLAIRE) in March 1998, J. Geophys. Res., 106, 14919–14934, doi:10.1029/2000JD900827, 2001. 4742

Formenti, P., Rajot, J. L., Desboeufs, K., Caquineau, S., Chevaillier, S., Nava, S., Gaudichet, A., Journet, E., Triquet, S., Alfaro, S., Chiari, M., Haywood, J., Coe, H., and Highwood, E.: Regional variability of the composition of mineral dust from western Africa: results from the AMMA SOP0/DABEX and DODO field campaigns, J. Geophys. Res., 113, D00C13, doi:10.1029/2008JD009903, 2008. 4740

Formenti, P., Schütz, L., Balkanski, Y., Desboeufs, K., Ebert, M., Kandler, K., Petzold, A., Scheuvens, D., Weinbruch, S., and Zhang, D.: Recent progress in understanding physical

ACPD
13, 4727–4784, 2013

and chemical properties of African and Asian mineral dust, Atmos. Chem. Phys., 11, 8231–8256, doi:10.5194/acp-11-8231-2011, 2011. 4734

Generoso, S., Bey, I., Labonne, M., and Breon, F.-M.: Aerosol vertical distribution in dust outflow over the Atlantic: comparisons between GEOS-Chem and Cloud-Aerosol Lidar and Infrared Pathfinder Satellite Observation (CALIPSO), J. Geophys. Res., 113, D24209, doi:10.1029/2008JD010154, 2008. 4732

Giglio, L., Csiszar, I., and Justice, C. O.: Global distribution and seasonality of active fires as observed with the Terra and Aqua Moderate Resolution Imaging Spectroradiometer (MODIS) sensors, J. Geophys. Res., 111, G02016, doi:10.1029/2005JG000142, 2006. 4740, 4741, 4743, 4745

Ginoux, P. and Torres, O.: Empirical TOMS index for dust aerosol: applications to model validation and source characterization, J. Geophys. Res., 108, 4534, doi:10.1029/2003JD003470, 2003. 4731

Gross, S., Tesche, M., Freudenthaler, V., Toledano, C., Wiegner, M., Ansmann, A., Althausen, D., and Seefeldner, M.: Characterization of Saharan dust, marine aerosols and mixtures of biomass-burning aerosols and dust by means of multi-wavelength depolarization and Raman lidar measurements during SAMUM 2, Tellus, 63, 706–724, doi:10.1111/j.1600-0889.2011.00556.x, 2011. 4739

Haywood, J. M., Pelon, J., Formenti, P., Bharmal, N., Brooks, M., Capes, G., Chazette, P., Chou, C., Christopher, S., Coe, H., Cuesta, J., Derimian, Y., Desboeufs, K., Greed, G., Harrison, M., Heese, B., Highwood, E. J., Johnson, B., Mallet, M., Marticorena, B., Marsham, J., Milton, S., Myhre, G., Osborne, S. R., Parker, D. J., Rajot, J.-L., Schulz, M., Slingo, A., Tanre, D., and Tulet, P.: Overview of the Dust and Biomass-burning Experiment and African Monsoon Multidisciplinary Analysis Special Observing Period-0, J. Geophys. Res., 113, D00C17, doi:10.1029/2008JD010077, 2008. 4739

Hu, Y., Li, D., and Liu, J.: Abrupt seasonal variation of the ITCZ and the Hadley circulation, Geophys. Res. Lett., 34, L18814, doi:10.1029/2007GL030950, 2007. 4751

Huang, J., Zhang, C., and Prospero, J. M.: African dust outbreaks: a satellite perspective of temporal and spatial variability over the tropical Atlantic Ocean, J. Geophys. Res., 115, D05202, doi:10.1029/2009JD012516, 2010. 4739, 4740, 4747

Immler, F. and Schrems, O.: Vertical profiles, optical and microphysical properties of Saharan dust layers determined by a ship-borne lidar, Atmos. Chem. Phys., 3, 1353–1364, doi:10.5194/acp-3-1353-2003, 2003. 4744

ACPD
13, 4727–4784, 2013

Ismail, S., Ferrare, R. A., Browell, E. V., Kooi, S. A., Dunion, J. P., Heymsfield, G., Notari, A., Butler, C. F., Burton, S., Fenn, M., Krishnamurti, T. N., Biswas, M. K., Chen, G., and Anderson, B.: LASE measurements of water vapor, aerosol, and cloud distributions in Saharan air layers and tropical disturbances, J. Atmos. Sci., 67, 1026–1047, doi:10.1175/2009JAS3136.1, 2010. 4744, 4753

Iwasaka, Y., Shibata, T., Nagatani, T., Shi, G.-Y., Kim, Y. S., Matsuki, A., Trochkine, D., Zhang, D., Yamada, M., Nagatani, M., Nakata, H., Shen, Z., Li, G., Chen, B., and Kawahira, K.: Large depolarization ratio of free tropospheric aerosols over the Taklamakan Desert revealed by lidar measurements: possible diffusion and transport of dust particles, J. Geophys. Res., 108, 8652, doi:10.1029/2002JD003267, 2003. 4734

Jenkins, G. S., Pratt, A. S., and Heymsfield, A.: Possible linkages between Saharan dust and tropical cyclone rain band invigoration in the eastern Atlantic during NAMMA-06, Geophys. Res. Lett., 35, L08815, doi:10.1029/2008GL034072, 2008. 4730

Jenkins, G. S., Robjhon, M. L., Smith, J. W., Clark, J., and Mendes, L.: The influence of the SAL and lightning on tropospheric ozone variability over the Northern Tropical Atlantic: results from Cape Verde during 2010, Geophys. Res. Lett., 39, L20810, doi:10.1029/2012GL053532, 2012. 4730

Jickells, T. D., An, Z. S., Andersen, K. K., Baker, A. R., Bergametti, G., Brooks, N., Cao, J. J., Boyd, P. W., Duce, R. A., Hunter, K. A., Kawahata, H., Kubilay, N., laRoche, J., Liss, P. S., Mahowald, N., Prospero, J. M., Ridgwell, A. J., Tegen, I., and Torres, R.: Global iron connections between desert dust, ocean biogeochemistry, and climate, Science, 308, 67–71, doi:10.1126/science.1105959, 2005. 4730

Johnson, B. T., Heese, B., McFarlane, S. A., Chazette, P., Jones, A., and Bellouin, N.: Vertical distribution and radiative effects of mineral dust and biomass burning aerosol over West Africa during DABEX, J. Geophys. Res., 113, D00C12, doi:10.1029/2008JD009848, 2008. 4740

Joseph, J. H., Yaron, O., Yaroslavich, E., Israelevich, P., Koren, I., Yair, Y., Devir, A., and Kischa, P.: Determination of most probable height of desert dust aerosol layer from space, J. Geophys. Res., 113, D20S93, doi:10.1029/2007JD009646, 2008. 4756

Kahn, R. A., Li, W.-H., Moroney, C., Diner, D. J., Martonchik, J. V., and Fishbein, E.: Aerosol source plume physical characteristics from space-based multiangle imaging, J. Geophys. Res., 112, D11205, doi:10.1029/2006JD007647, 2007. 4756

ACPD
13, 4727–4784, 2013

Kalashnikova, O. V. and Kahn, R. A.: Mineral dust plume evolution over the Atlantic from MISR and MODIS aerosol retrievals, J. Geophys. Res., 113, D24204, doi:10.1029/2008JD010083, 2008. 4736, 4738

Karyampudi, V. M., Palm, S. P., Reagen, J. A., Fang, H., Grant, W. B., Hoff, R. M., Moulin, C., Pierce, H. F., Torres, O., Browell, E. V., and Melfi, S. H.: Validation of the Saharan dust plume conceptual model using lidar, Meteosat, and ECMWF data, B. Am. Meteorol. Soc., 80, 1045–1075, doi:10.1175/1520-0477(1999)080<1045:VOTSDP>2.0.CO;2, 1999. 4729, 4742, 4746, 4750, 4752, 4754

Kaufman, Y. J., Koren, I., Remer, L. A., Tanre, D., Ginoux, P., and Fan, S.: Dust transport and deposition observed from the Terra-Moderate Resolution Imaging Spectroradiometer (MODIS) spacecraft over the Atlantic Ocean, J. Geophys. Res., 110, D10S12, doi:10.1029/2003JD004436, 2005. 4730, 4736, 4740

Kittaka, C., Winker, D. M., Vaughan, M. A., Omar, A., and Remer, L. A.: Intercomparison of column aerosol optical depths from CALIPSO and MODIS-Aqua, Atmos. Meas. Tech., 4, 131–141, doi:10.5194/amt-4-131-2011, 2011. 4735

Knippertz, P., Tesche, M., Heinold, B., Kandler, K., Toledano, C., and Esselborn, M.: Dust mobilization and aerosol transport from West Africa to Cape Verde – a meteorological overview of SAMUM-2, Tellus, 63, 430–447, doi:10.1111/j.1600-0889.2011.00544.x, 2011. 4734

Koffi, B., Schulz, M., Breon, F.-M., Griesfeller, J., Winker, D., Balkanski, Y., Bauer, S., Berntsen, T., Chin, M., Collins, W. D., Dentener, F., Diehl, T., Easter, R., Ghan, S., Ginoux, P., Gong, S., Horowitz, L. W., Iversen, T., Kirkevag, A., Koch, D., Krol, M., Myhre, G., Stier, P., and Takemura, T.: Application of the CALIOP layer product to evaluate the vertical distribution of aerosols estimated by global models: AeroCom phase I results, J. Geophys. Res., 117, D10201, doi:10.1029/2011JD016858, 2012. 4755

Kokhanovsky, A. A. and Rozanov, V. V.: The determination of dust cloud altitudes from a satellite using hyperspectral measurements in the gaseous absorption band, Int. J. Remote Sens., 31, 2729–2744, doi:10.1080/01431160903085644, 2010. 4756

Koren, I., Kaufman, Y. J., Washington, R., Todd, M. C., Rudich, Y., Martins, J. V., and Rosenfeld, D.: The Bodélé depression: a single spot in the Sahara that provides most of the mineral dust to the Amazon forest, Environmental Research Letters, 1, 014005, doi:10.1088/1748-9326/1/1/014005, 2006. 4740

Lafore, J.-P., Flamant, C., Guichard, F., Parker, D. J., Bouniol, D., Fink, A. H., Giraud, V., Gosset, M., Hall, N., Holler, H., Jones, S. C., Protat, A., Roca, R., Roux, F., Said, F., and

ACPD
13, 4727–4784, 2013

Thorncroft, C.: Progress in understanding of weather systems in West Africa, Atmos. Sci. Lett., 12, 7–12, doi:10.1002/asl.335, 2011. 4752, 4753

Lau, K. M. and Kim, K. M.: Cooling of the Atlantic by Saharan dust, Geophys. Res. Lett., 34, L23811, doi:10.1029/2007GL031538, 2007. 4730

Léon, J.-F., Derimian, Y., Chiapello, I., Tanré, D., Podvin, T., Chatenet, B., Diallo, A., and Deroo, C.: Aerosol vertical distribution and optical properties over M'Bour (16.96° W; 14.39° N), Senegal from 2006 to 2008, Atmos. Chem. Phys., 9, 9249–9261, doi:10.5194/acp-9-9249-2009, 2009. 4741, 4745

Liao, H. and Seinfeld, J. H.: Radiative forcing by mineral dust aerosols: sensitivity to key variables, J. Geophys. Res., 103, 31637–31645, doi:10.1029/1998JD200036, 1998. 4731

Liu, D., Wang, Z., Liu, Z., Winker, D., and Trepte, C.: A height resolved global view of dust aerosols from the first year CALIPSO lidar measurements, J. Geophys. Res., 113, D16214, doi:10.1029/2007JD009776, 2008a. 4732

Liu, Z., Omar, A., Vaughan, M., Hair, J., Kittaka, C., Hu, Y., Powell, K., Trepte, C., Winker, D., Hostetler, C., Ferrare, R., and Pierce, R.: CALIPSO lidar observations of the optical properties of Saharan dust: a case study of long-range transport, J. Geophys. Res., 113, D07207, doi:10.1029/2007JD008878, 2008b. 4732, 4742, 4746

Liu, Z., Vaughan, M. A., Winker, D. M., Kittaka, C., Getzewich, B., Kuehn, R., Omar, A., Powell, K., Trepte, C., and Hostetler, C.: The CALIPSO lidar cloud and aerosol discrimination: version 2 algorithm and initial assessment of performance, J. Atmos. Ocean. Tech., 26, 1198–1213, doi:10.1175/2009JTECHA1229.1, 2009. 4733

Liu, Z., Kuehn, R., Vaughan, M., Winker, D., Omar, A., Powell, K., Trepte, C., Hu, Y., and Hostetler, C.: The CALIPSO cloud and aerosol discrimination: version 3 algorithm and test results, in: 25th International Laser Radar Conference (ILRC), St. Petersburg, Russia, 5–9 July, 2010. 4733

Maddy, E. S., DeSouza-Machado, S. G., Nalli, N. R., Barnet, C. D., Strow, L. L., Wolf, W. W., Xie, H., Gambacorta, A., King, T. S., Joseph, E., Morris, V., Hannon, S. E., and Schou, P.: On the effect of dust aerosols on AIRS and IASI operational level 2 products, Geophys. Res. Lett., 39, L10809, doi:10.1029/2012GL052070, 2012. 4731

Maher, B. A., Prospero, J. M., Mackie, D., Gaiero, D., Hesse, P. P., and Balkanski, Y.: Global connections between aeolian dust, climate and ocean biogeochemistry at the present day and at the last glacial maximum, Earth-Sci. Rev., 99, 61–97, doi:10.1016/j.earscirev.2009.12.001, 2010. 4737

ACPD
13, 4727–4784, 2013

Mahowald, N. M. and Kiehl, L. M.: Mineral aerosol and cloud interactions, Geophys. Res. Lett., 30, 1475, doi:10.1029/2002GL016762, 2003. 4730

Maring, H., Savoie, D. L., Izaguirre, M. A., Custals, L., and Reid, J. S.: Mineral dust aerosol size distribution change during atmospheric transport, J. Geophys. Res., 108, 8592, doi:10.1029/2002JD002536, 2003. 4748

Marticorena, B., Haywood, J., Coe, H., Formenti, P., Liousse, C., Mallet, M., and Pelon, J.: Tropospheric aerosols over West Africa: highlights from the AMMA international program, Atmos. Sci. Lett., 12, 19–23, doi:10.1002/asl.322, 2011. 4751

Mattis, I., Ansmann, A., Muller, D., Wandinger, U., and Althausen, D.: Dual-wavelength Raman lidar observations of the extinction-to-backscatter ratio of Saharan dust, Geophys. Res. Lett., 29, doi:10.1029/2002GL014721, 2002. 4735

McConnell, C. L., Highwood, E. J., Coe, H., Formenti, P., Anderson, B., Osborne, S., Nava, S., Desboeufs, K., Chen, G., and Harrison, M. A. J.: Seasonal variations of the physical and optical characteristics of Saharan dust: results from the Dust Outflow and Deposition to the Ocean (DODO) experiment, J. Geophys. Res., 113, D14S05, doi:10.1029/2007JD009606, 2008. 4740, 4744

Meloni, D., di Sarra, A., Di Iorio, T., and Fiocco, G.: Influence of the vertical profile of Saharan dust on the visible direct radiative forcing, J. Quant. Spectrosc. Ra., 93, 397–413, doi:10.1016/j.jqsrt.2004.08.035, 2005. 4731

Mielonen, T., Arola, A., Komppula, M., Kukkonen, J., Koskinen, J., de Leeuw, G., and Lehtinen, K. E. J.: Comparison of CALIOP level 2 aerosol subtypes to aerosol types derived from AERONET inversion data, Geophys. Res. Lett., 36, L18804, doi:10.1029/2009GL039609, 2009. 4734

Muller, D., Ansmann, A., Mattis, I., Tesche, M., Wandinger, U., Althausen, D., and Pisani, G.: Aerosol-type-dependent lidar ratios observed with Raman lidar, J. Geophys. Res., 112, D16202, doi:10.1029/2006JD008292, 2007. 4735

Nalli, N. R., Clemente-Colon, P., Morris, V., Joseph, E., Szczodrak, M., Minnett, P. J., Shannahoff, J., Goldberg, M. D., Barnet, C., Wolf, W. W., Feltz, W. F., and Knuteson, R. O.: Profile observations of the Saharan air layer during AEROSE 2004, Geophys. Res. Lett., 32, L05815, doi:10.1029/2004GL022028, 2005. 4756

Nalli, N. R., Joseph, E., Morris, V. R., Barnet, C. D., Wolf, W. W., Wolfe, D., Minnett, P. J., Szczodrak, M., Izaguirre, M. A., Lumpkin, R., Xie, H., Smirnov, A., King, T. S., and Wei, J.: Multiyear observations of the tropical Atlantic atmosphere: multidisciplinary applications of

ACPD
13, 4727–4784, 2013

the NOAA aerosols and ocean science expeditions, B. Am. Meteorol. Soc., 92, 765–789, doi:10.1175/2011BAMS2997.1, 2011. 4754, 4756

Noll, K. E. and Aluko, O.: Changes in large particle size distribution due to dry deposition processes, J. Aerosol Sci., 37, 1797–1808, doi:10.1016/j.jaerosci.2006.08.006, 2006. 4748

Omar, A. H., Winker, D. M., Kittaka, C., Vaughan, M. A., Liu, Z., Hu, Y., Trepte, C. R., Rogers, R. R., Ferrare, R. A., Lee, K.-P., Kuehn, R. E., and Hostetler, C. A.: The CALIPSO automated aerosol classification and lidar ratio selection algorithm, J. Atmos. Ocean. Tech., 26, 1994–2014, doi:10.1175/2009JTECHA1231.1, 2009. 4734, 4739

Peyridieu, S., Chédin, A., Tanré, D., Capelle, V., Pierangelo, C., Lamquin, N., and Armante, R.: Saharan dust infrared optical depth and altitude retrieved from AIRS: a focus over North Atlantic – comparison to MODIS and CALIPSO, Atmos. Chem. Phys., 10, 1953–1967, doi:10.5194/acp-10-1953-2010, 2010. 4731, 4736, 4756

Peyridieu, S., Chédin, A., Capelle, V., Tsamalis, C., Pierangelo, C., Armante, R., Crevoisier, C., Crépeau, L., Siméon, M., Ducos, F., and Scott, N. A.: Characterization of dust aerosols in the infrared from IASI and comparison with PARASOL, MODIS, MISR, CALIOP, and AERONET observations, Atmos. Chem. Phys. Discuss., 12, 23093–23133, doi:10.5194/acpd-12-23093-2012, 2012. 4731, 4736, 4756

Pierangelo, C., Chédin, A., Heilliette, S., Jacquinet-Husson, N., and Armante, R.: Dust altitude and infrared optical depth from AIRS, Atmos. Chem. Phys., 4, 1813–1822, doi:10.5194/acp-4-1813-2004, 2004. 4731

Prenni, A. J., Petters, M. D., Kreidenweis, S. M., Heald, C. L., Martin, S. T., Artaxo, P., Garland, R. M., Wollny, A. G., and Poschl, U.: Relative roles of biogenic emissions and Saharan dust as ice nuclei in the Amazon basin, Nat. Geosci., 2, 402–405, doi:10.1038/NGEO517, 2009. 4740

Prospero, J. M. and Lamb, P. J.: African droughts and dust transport to the Caribbean: climate change implications, Science, 302, 1024–1027, doi:10.1126/science.1089915, 2003. 4731

Prospero, J. M., Glaccum, R. A., and Nees, R. T.: Atmospheric transport of soil dust from Africa to South America, Nature, 289, 570–572, doi:10.1038/289570a0, 1981. 4742

Prospero, J. M., Landing, W. M., and Schulz, M.: African dust deposition to Florida: temporal and spatial variability and comparisons to models, J. Geophys. Res., 115, D13304, doi:10.1029/2009JD012773, 2010. 4748

ACPD
13, 4727–4784, 2013

Prospero, J. M., Bullard, J. E., and Hodgkins, R.: High-latitude dust over the North Atlantic: inputs from Icelandic proglacial dust storms, Science, 335, 1078–1082, doi:10.1126/science.1217447, 2012. 4754

Quijano, A. L., Sokolik, I. N., and Toon, O. B.: Influence of the aerosol vertical distribution on the retrievals of aerosol optical depth from satellite radiance measurements, Geophys. Res. Lett., 27, 3457–3460, doi:10.1029/1999GL011235, 2000. 4731

Redemann, J., Vaughan, M. A., Zhang, Q., Shinozuka, Y., Russell, P. B., Livingston, J. M., Kacenelenbogen, M., and Remer, L. A.: The comparison of MODIS-Aqua (C5) and CALIOP (V2 & V3) aerosol optical depth, Atmos. Chem. Phys., 12, 3025–3043, doi:10.5194/acp-12-3025-2012, 2012. 4735

Reid, J. S., Westphal, D. L., Livingston, J. M., Savoie, D. L., Maring, H. B., Jonsson, H. H., Eleuterio, D. P., Kinney, J. E., and Reid, E. A.: Dust vertical distribution in the Caribbean during the Puerto Rico Dust experiment, Geophys. Res. Lett., 29, 1151, doi:10.1029/2001GL014092, 2002. 4731, 4744

Reid, J. S., Kinney, J. E., Westphal, D. L., Holben, B. N., Welton, E. J., Tsay, S.-C., Eleuterio, D. P., Campbell, J. R., Christopher, S. A., Colarco, P. R., Jonsson, H. H., Livingston, J. M., Maring, H. B., Meier, M. L., Pilewskie, P., Prospero, J. M., Reid, E. A., Remer, L. A., Russell, P. B., Savoie, D. L., Smirnov, A., and Tanre, D.: Analysis of measurements of Saharan dust by airborne and groundbased remote sensing methods during the Puerto Rico Dust Experiment (PRIDE), J. Geophys. Res., 108, 8586, doi:10.1029/2002JD002493, 2003. 4744

Remer, L. A., Kaufman, Y. J., Tanre, D., Matoo, S., Chu, D. A., Martins, J. V., Li, R.-R., Ichoku, C., Levy, R. C., Kleidman, R. G., Eck, T. F., Vermote, E., and Holben, B. N.: The MODIS aerosol algorithm, products, and validation, J. Atmos. Sci., 62, 947–973, doi:10.1175/JAS3385.1, 2005. 4736

Remer, L. A., Kleidman, R. G., Levy, R. C., Kaufman, Y. J., Tanre, D., Mattoo, S., Martins, J. V., Ichoku, C., Koren, I., Yu, H., and Holben, B. N.: Global aerosol climatology from the MODIS satellite sensors, J. Geophys. Res., 113, D14S07, doi:10.1029/2007JD009661, 2008. 4736

Ridley, D. A., Heald, C. L., and Ford, B.: North African dust export and deposition: a satellite and model perspective, J. Geophys. Res., 117, D02202, doi:10.1029/2011JD016794, 2012. 4732

Rodríguez, S., Alastuey, A., Alonso-Pérez, S., Querol, X., Cuevas, E., Abreu-Afonso, J., Viana, M., Pérez, N., Pandolfi, M., and de la Rosa, J.: Transport of desert dust mixed with

ACPD
13, 4727–4784, 2013

North African industrial pollutants in the subtropical Saharan Air Layer, Atmos. Chem. Phys., 11, 6663–6685, doi:10.5194/acp-11-6663-2011, 2011. 4734
Sassen, K., DeMott, P. J., Prospero, J. M., and Poellot, M. R.: Saharan dust storms and indirect aerosol effects on clouds: CRYSTAL-FACE results, Geophys. Res. Lett., 30, 1633, doi:10.1029/2003GL017371, 2003. 4744
Schepanski, K., Tegen, I., and Macke, A.: Saharan dust transport and deposition towards the tropical northern Atlantic, Atmos. Chem. Phys., 9, 1173–1189, doi:10.5194/acp-9-1173-2009, 2009. 4731, 4749, 4751
Schuster, G. L., Vaughan, M., MacDonnell, D., Su, W., Winker, D., Dubovik, O., Lapyonok, T., and Trepte, C.: Comparison of CALIPSO aerosol optical depth retrievals to AERONET measurements, and a climatology for the lidar ratio of dust, Atmos. Chem. Phys., 12, 7431–7452, doi:10.5194/acp-12-7431-2012, 2012. 4735
Shell, K. M. and Somerville, R. C. J.: Sensitivity of climate forcing and response to dust optical properties in an idealized model, J. Geophys. Res., 112, D03206, doi:10.1029/2006JD007198, 2007. 4731
Smirnov, A., Holben, B. N., Giles, D. M., Slutsker, I., O'Neill, N. T., Eck, T. F., Macke, A., Croot, P., Courcoux, Y., Sakerin, S. M., Smyth, T. J., Zielinski, T., Zibordi, G., Goes, J. I., Harvey, M. J., Quinn, P. K., Nelson, N. B., Radionov, V. F., Duarte, C. M., Losno, R., Sciare, J., Voss, K. J., Kinne, S., Nalli, N. R., Joseph, E., Krishna Moorthy, K., Covert, D. S., Gulev, S. K., Milinevsky, G., Larouche, P., Belanger, S., Horne, E., Chin, M., Remer, L. A., Kahn, R. A., Reid, J. S., Schulz, M., Heald, C. L., Zhang, J., Lapina, K., Kleidman, R. G., Griesfeller, J., Gaitley, B. J., Tan, Q., and Diehl, T. L.: Maritime aerosol network as a component of AERONET – first results and comparison with global aerosol models and satellite retrievals, Atmos. Meas. Tech., 4, 583–597, doi:10.5194/amt-4-583-2011, 2011. 4738, 4744
Sun, D., Lau, K. M., and Kafatos, M.: Contrasting the 2007 and 2005 hurricane seasons: evidence of possible impacts of Saharan dry air and dust on tropical cyclone activity in the Atlantic basin, Geophys. Res. Lett., 35, L15405, doi:10.1029/2008GL034529, 2008. 4730
Tesche, M., Gross, S., Ansmann, A., Muller, D., Althausen, D., Freudenthaler, V., and Esselborn, M.: Profiling of Saharan dust and biomass-burning smoke with multiwavelength polarization Raman lidar at Cape Verde, Tellus, 63, 649–676, doi:10.1111/j.1600-0889.2011.00548.x, 2011. 4740, 4744

ACPD
13, 4727–4784, 2013

Thorsen, T. J., Fu, Q., and Comstock, J.: Comparison of the CALIPSO satellite and ground-based observations of cirrus clouds at the ARM TWP sites, J. Geophys. Res., 116, D21203, doi:10.1029/2011JD015970, 2011. 4733

Tompkins, A. M., Cardinali, C., Morcrette, J.-J., and Rodwell, M.: Influence of aerosol climatology on forecasts of the African Easterly Jet, Geophys. Res. Lett., 32, L10801, doi:10.1029/2004GL022189, 2005. 4753

Torres, O., Tanskanen, A., Veihelmann, B., Ahn, C., Braak, R., Bhartia, P. K., Veefkind, P., and Levelt, P.: Aerosols and surface UV products from Ozone Monitoring Instrument observations: an overview, J. Geophys. Res., 112, D24S47, doi:10.1029/2007JD008809, 2007. 4731

Twohy, C. H., Kreidenweis, S. M., Eidhammer, T., Browell, E. V., Heymsfield, A. J., Bansemer, A. R., Anderson, B. E., Chen, G., Ismail, S., DeMott, P. J., and Van Den Heever, S. C.: Saharan dust particles nucleate droplets in eastern Atlantic clouds, Geophys. Res. Lett., 36, L01807, doi:10.1029/2008GL035846, 2009. 4730

Uno, I., Eguchi, K., Yumimoto, K., Takemura, T., Shimizu, A., Uematsu, M., Liu, Z., Wang, Z., Hara, Y., and Sugimoto, N.: Asian dust transported one full circuit around the globe, Nat. Geosci., 2, 557–560, 2009. 4741

van der Werf, G. R., Randerson, J. T., Collatz, G. J., and Giglio, L.: Carbon emissions from fires in tropical and subtropical ecosystems, Glob. Change Biol., 9, 547–562, doi:10.1046/j.1365-2486.2003.00604.x, 2003. 4740, 4741, 4745

Vaughan, M. A., Powell, K. A., Kuehn, R. E., Young, S. A., Winker, D. M., Hostetler, C. A., Hunt, W. H., Liu, Z., McGill, M. J., and Getzewich, B. J.: Fully automated detection of cloud and aerosol layers in the CALIPSO lidar measurements, J. Atmos. Ocean. Tech., 26, 2034–2050, doi:10.1175/2009JTECHA1228.1, 2009. 4733

Voss, K. J., Welton, E. J., Quinn, P. K., Johnson, J., Thompson, A. M., and Gordon, H. R.: Lidar measurements during Aerosols99, J. Geophys. Res., 106, 20821–20831, doi:10.1029/2001JD900217, 2001. 4740

Waliser, D. E. and Gautier, C.: A satellite-derived climatology of the ITCZ, J. Climate, 6, 2162–2174, doi:10.1175/1520-0442(1993)006<2162:ASDCOT>2.0.CO;2, 1993. 4751, 4752

Wang, K.-Y.: Profiles of the atmospheric temperature response to the Saharan dust outbreaks derived from FORMOSAT-3/COSMIC and OMI AI, Atmos. Res., 96, 110–121, doi:10.1016/j.atmosres.2009.11.017, 2009. 4729, 4743

Wilcox, E. M., Lau, K. M., and Kim, K.-M.: A northward shift of the North Atlantic Ocean Intertropical Convergence Zone in response to summertime Saharan dust outbreaks, Geophys. Res. Lett., 37, L04804, doi:10.1029/2009GL041774, 2010. 4730, 4742, 4753

Winker, D. M., Hunt, W. H., and McGill, M. J.: Initial performance assessment of CALIOP, Geophys. Res. Lett., 34, L19803, doi:10.1029/2007GL030135, 2007. 4731, 4732

Winker, D. M., Vaughan, M. A., Omar, A., Hu, Y., Powell, K. A., Liu, Z., Hunt, W. H., and Young, S. A.: Overview of the CALIPSO mission and CALIOP data processing algorithms, J. Atmos. Ocean. Tech., 26, 2310–2323, doi:10.1175/2009JTECHA1281.1, 2009. 4732

Winker, D. M., Pelon, J., Coakley Jr., J. A., Ackerman, S. A., Charlson, R. J., Colarco, P. R., Flamant, P., Fu, Q., Hoff, R. M., Kittaka, C., Kubar, T. L., Le Treut, H., McCormick, M. P., Megie, G., Poole, L., Powell, K., Trepte, C., Vaughan, M. A., and Wielicki, B. A.: The CALIPSO mission: a global 3D view of aerosols and clouds, B. Am. Meteorol. Soc., 91, 1211–1229, doi:10.1175/2010BAMS3009.1, 2010. 4734, 4735

Wong, S. and Dessler, A. E.: Suppression of deep convection over the tropical North Atlantic by the Saharan Air Layer, Geophys. Res. Lett., 32, L09808, doi:10.1029/2004GL022295, 2005. 4730, 4736

Wong, S., Dessler, A. E., Mahowald, N. M., Yang, P., and Feng, Q.: Maintenance of lower tropospheric temperature inversion in the Saharan Air Layer by dust and dry anomaly, J. Climate, 22, 5149–5162, doi:10.1175/2009JCLI2847.1, 2009. 4729

Wu, D. L., Chae, J. H., Lambert, A., and Zhang, F. F.: Characteristics of CALIOP attenuated backscatter noise: implication for cloud/aerosol detection, Atmos. Chem. Phys., 11, 2641–2654, doi:10.5194/acp-11-2641-2011, 2011. 4735

Wu, L.: Impact of Saharan air layer on hurricane peak intensity, Geophys. Res. Lett., 34, L09802, doi:10.1029/2007GL029564, 2007. 4730

Wu, M.-L. C., Reale, O., Schubert, S. D., Suarez, M. J., Koster, R. D., and Pegion, P. J.: African Easterly Jet: structure and maintenance, J. Climate, 22, 4459–4480, doi:10.1175/2009JCLI2584.1, 2009. 4752

Yang, W., Marshak, A., Várnai, T., Kalashnikova, O. V., and Kostinski, A. B.: CALIPSO observations of transatlantic dust: vertical stratification and effect of clouds, Atmos. Chem. Phys., 12, 11339–11354, doi:10.5194/acp-12-11339-2012, 2012. 4732, 4734

Yu, H., Chin, M., Winker, D. M., Omar, A. H., Liu, Z., Kittaka, C., and Diehl, T.: Global view of aerosol vertical distributions from CALIPSO lidar measurements and

ACPD
13, 4727–4784, 2013

GOCART simulations: regional and seasonal variations, J. Geophys. Res., 115, D00H30, doi:10.1029/2009JD013364, 2010. 4732
Zagar, N., Skok, G., and Tribbia, J.: Climatology of the ITCZ derived from ERA Interim reanalyses, J. Geophys. Res., 116, D15103, doi:10.1029/2011JD015695, 2011. 4751
Zhang, C. and Pennington, J.: African dry air outbreaks, J. Geophys. Res., 109, D20108, doi:10.1029/2003JD003978, 2004. 4756
Zhang, J. and Zhang, Q.: Aerosol impact and correction on temperature profile retrieval from MODIS, Geophys. Res. Lett., 35, L13818, doi:10.1029/2008GL034419, 2008. 4731
Zhu, A., Ramanathan, V., Li, F., and Kim, D.: Dust plumes over the Pacific, Indian, and Atlantic oceans: climatology and radiative impact, J. Geophys. Res., 112, D16208, doi:10.1029/2007JD008427, 2007. 4731, 4744, 4746, 4754
Zipser, E. J., Twohy, C. H., Tsay, S.-C., Lee Thornhill, K., Tanelli, S., Ross, R., Krishnamurti, T. N., Ji, Q., Jenkins, G., Ismail, S., Hsu, N. C., Hood, R., Heymsfield, G. M., Heymsfield, A., Halverson, J., Goodman, H. M., Ferrare, R., Dunion, J. P., Douglas, M., Cifelli, R., Chen, G., Browell, E. V., and Anderson, B.: The Saharan Air Layer and the fate of African Easterly Waves-NASA's AMMA field study of tropical cyclogenesis, B. Am. Meteorol. Soc., 90, 1137–1156, doi:10.1175/2009BAMS2728.1, 2009. 4730, 4753, 4754

ACPD
13, 4727–4784, 2013

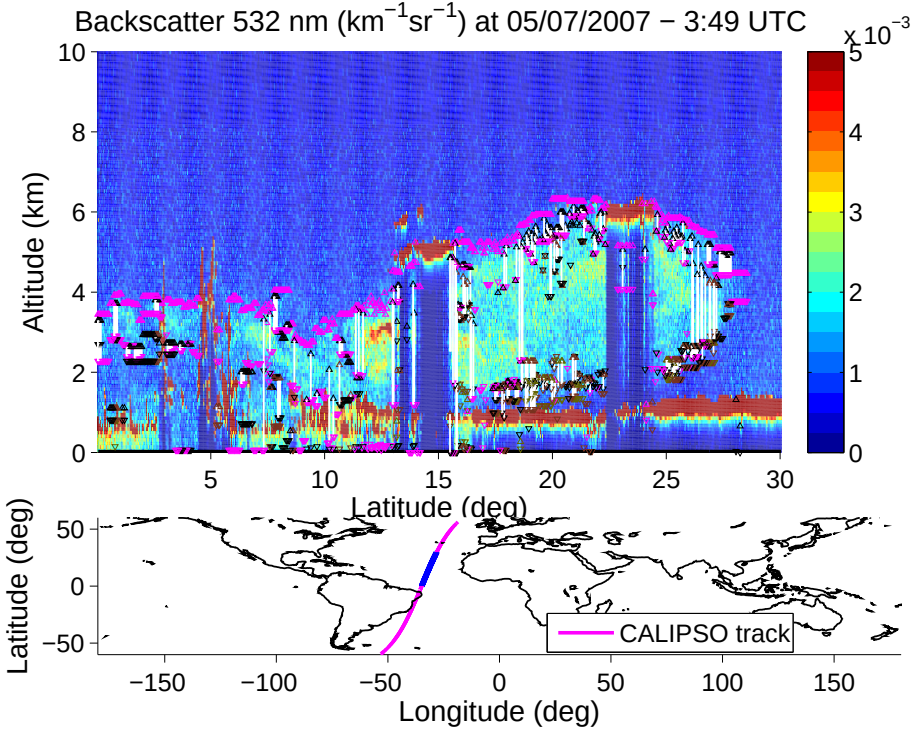

Fig. 1. An example of SAL as observed from CALIOP on 5 July 2007 at 3:49 UTC. Top: the latitude-altitude cross section of the attenuated backscatter coefficient at 532 µm (km^{-1}sr^{-1}). The brown features at about 1 km and the elevated ones at about 5°, 15° and 22° N are clouds. The white lines mark the overlap (see text for details) and the triangles (magenta, black or brown) show the top and the base of dust layers as detected by CALIPSO. Bottom: the CALIPSO track, with the part of the cross section presented above highlighted in blue.

ACPD
13, 4727–4784, 2013

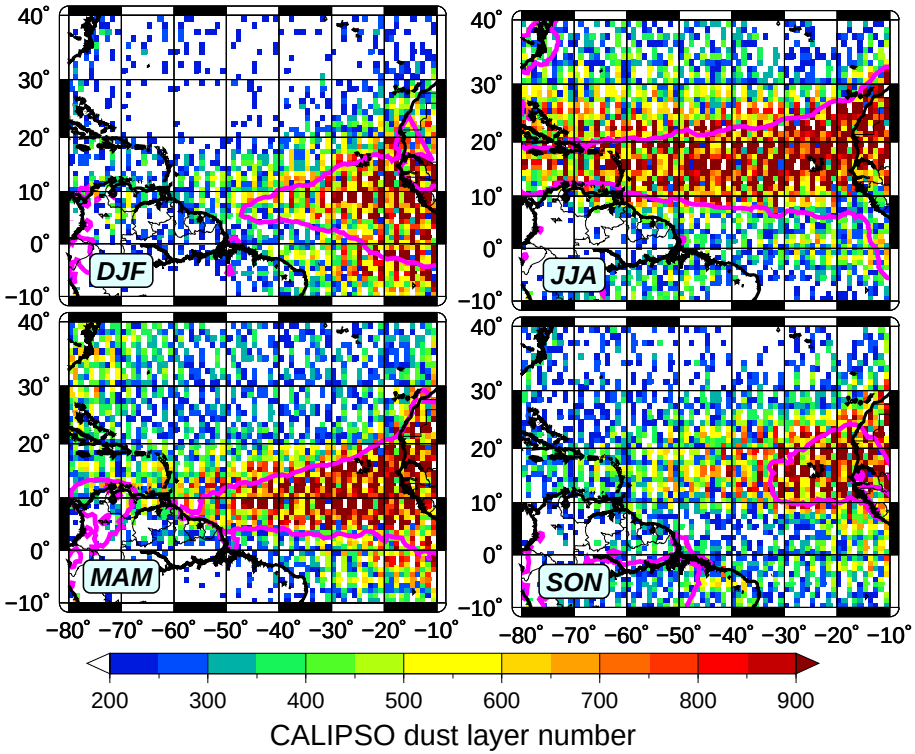

Fig. 2. Number of dust layers (desert dust and polluted dust) detected by CALIPSO above the Atlantic during 5-yr period June 2006 to May 2011 for the four seasons: winter (DJF – top left), spring (MAM – bottom left), summer (JJA – top right) and fall (SON – bottom right). The magenta lines are the 0.25 AOD isolines from MODIS for each season.

ACPD
13, 4727–4784, 2013

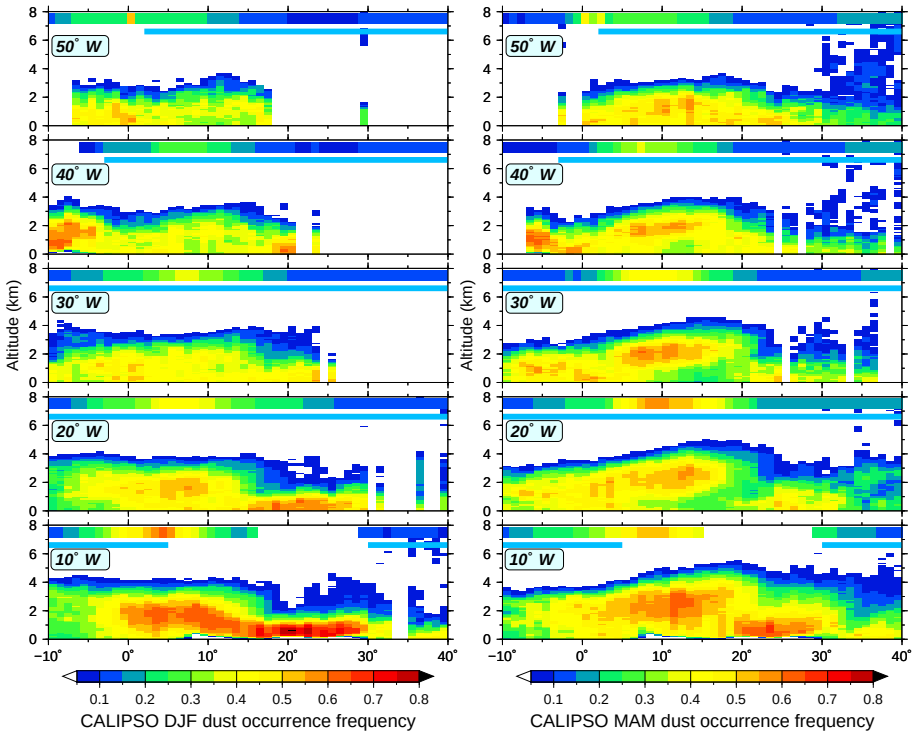

Fig. 3. Vertical distribution of the dust aerosols occurrence frequency above the Atlantic Ocean at five longitudes (10° W, 20° W, 30° W, 40° W and 50° W) during winter (DJF – left) and spring (MAM – right) seasons from 5 yr of CALIPSO observations. The abscissa is the latitude from 10° S to 40° N. The cyan line at 6.5 km of each cross section marks the ocean, while the colour line above it, between 7 and 8 km, is the MODIS AOD at 550 nm. The colorbar of MODIS AOD is the same as that of the dust occurrence frequency.

ACPD
13, 4727–4784, 2013

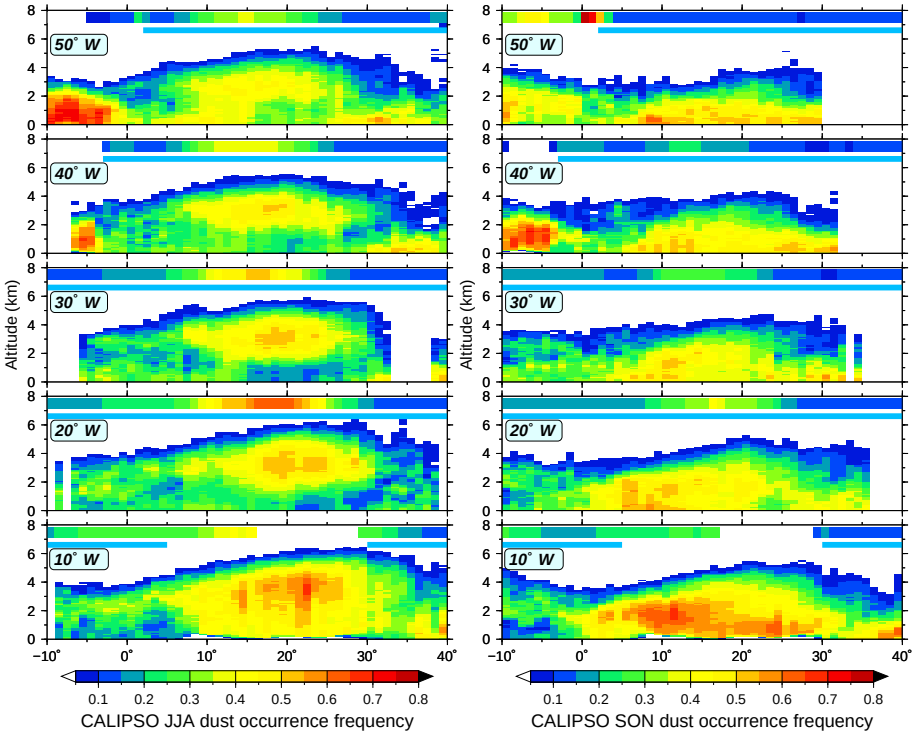

Fig. 4. Same as Fig. 3 but for summer (JJA – left) and fall (SON – right) seasons.

ACPD
13, 4727–4784, 2013

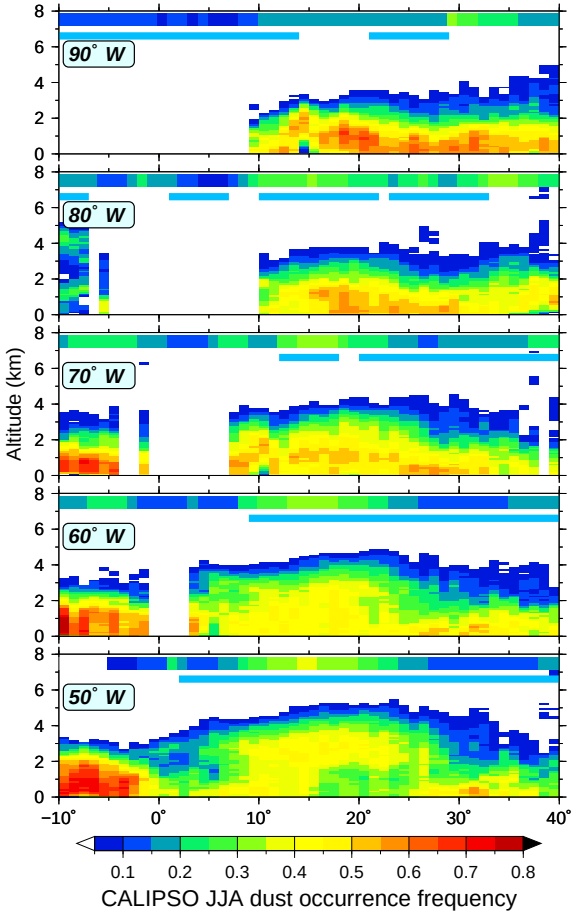

Fig. 5. Same as Fig. 3 but only for summer (JJA) at the five longitudes: 50° W, 60° W, 70° W, 80° W and 90° W. The cross section at 50° W is repeated in order to facilitate the inspection of SAL evolution.

ACPD
13, 4727–4784, 2013

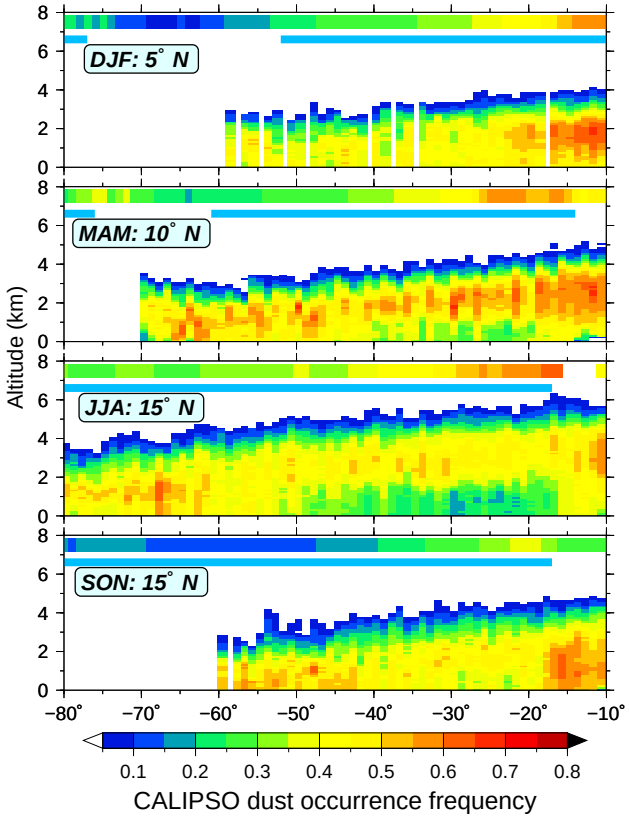

Fig. 6. Vertical distribution of the dust aerosols occurrence frequency above the Atlantic Ocean (from top to bottom) during winter (DJF at 5° N), spring (MAM at 10° N), summer (JJA at 15° N) and fall (SON at 15° N). The abscissa is the longitude from 80° W to 10° W. The cyan line at 6.5 km of each cross section marks the ocean, while the colour line above it, between 7 and 8 km, is the MODIS AOD at 550 nm. The colorbar of MODIS AOD is the same as that of the dust occurrence frequency.

ACPD
13, 4727–4784, 2013

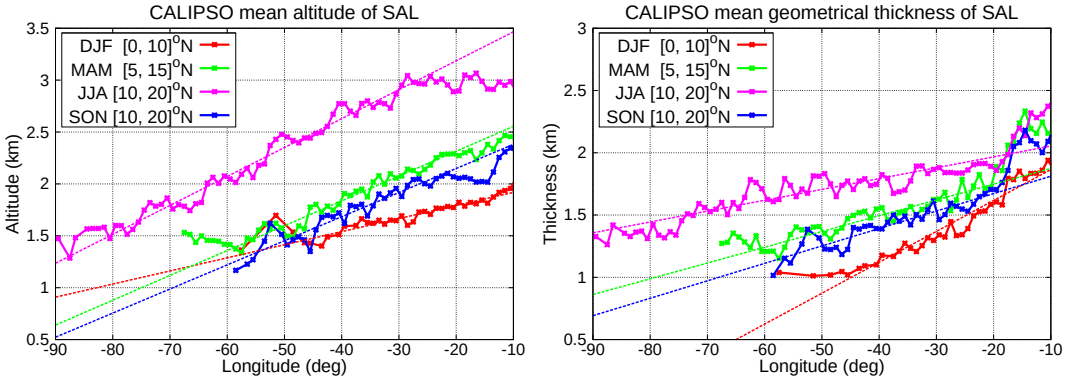

Fig. 7. Mean zonal evolution of SAL altitude (left) and geometrical thickness (right) based on CALIPSO data from Africa (−10° E) to America (−90° E). Each point is an average over 10° in latitude (indicated in the legend) depicting the mainly position of SAL in every season. The dotted lines are the linear fits for every season (see text for details).

ACPD
13, 4727–4784, 2013

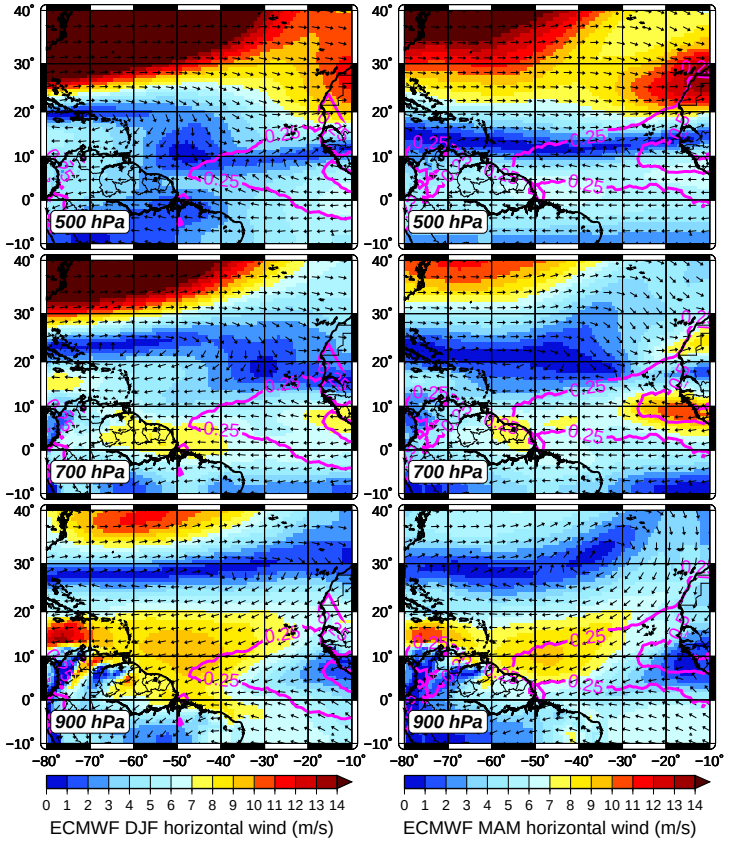

Fig. 8. Horizontal wind from ECMWF at three pressure levels (900 hPa – bottom, 700 hPa – middle and 500 hPa – top) during winter (DJF – left) and spring (MAM-right) seasons averaged over the same period as for CALIPSO. The vectors indicate the direction and the colour the wind speed ($m\,s^{-1}$). The magenta isolines of 0.25 and 0.5 depict the MODIS AOD at 550 nm.

ACPD
13, 4727–4784, 2013

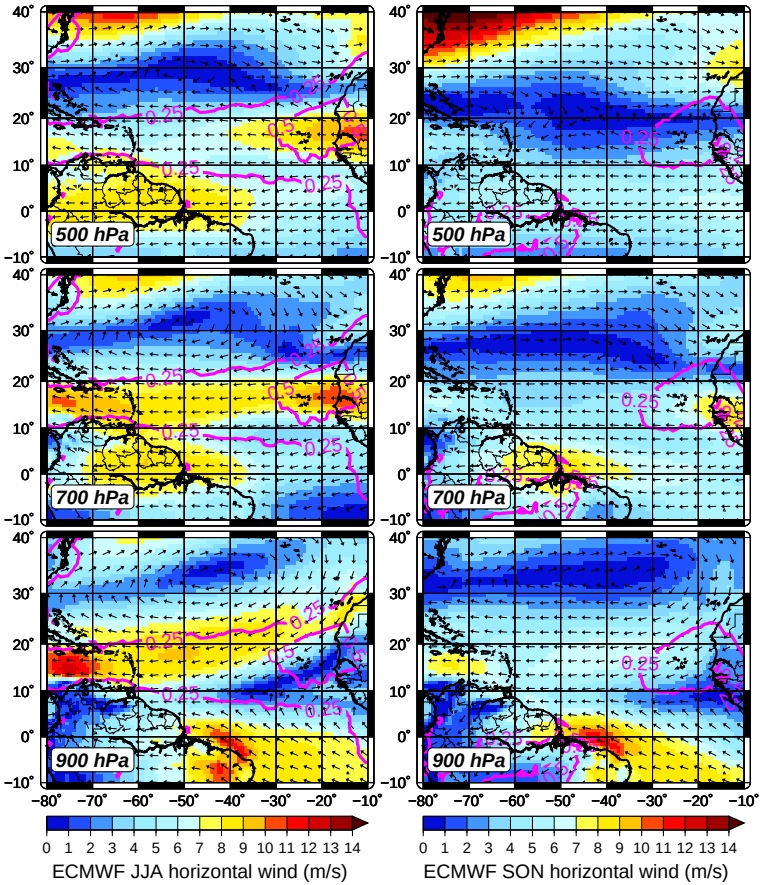

Fig. 9. Same as Fig. 8 but for summer (JJA – left) and fall (SON – right) seasons.

ACPD
13, 4727–4784, 2013

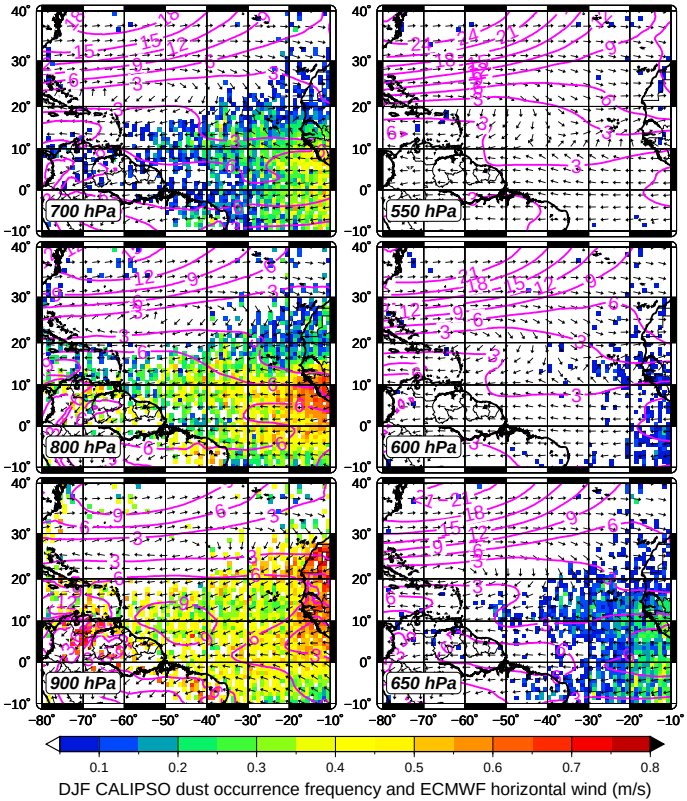

Fig. A1. CALIPSO dust occurrence frequency at 6 pressure levels (colorscale): 900 hPa (left-bottom), 800 hPa (left-middle), 700 hPa (left-top), 650 hPa (right-bottom), 600 hPa (right-middle) and 550 hPa (right-top). The black vectors show the horizontal wind direction from ECMWF reanalysis and the magenta isolines the wind speed ($m\,s^{-1}$) with a step of $3\,m\,s^{-1}$.

ACPD
13, 4727–4784, 2013

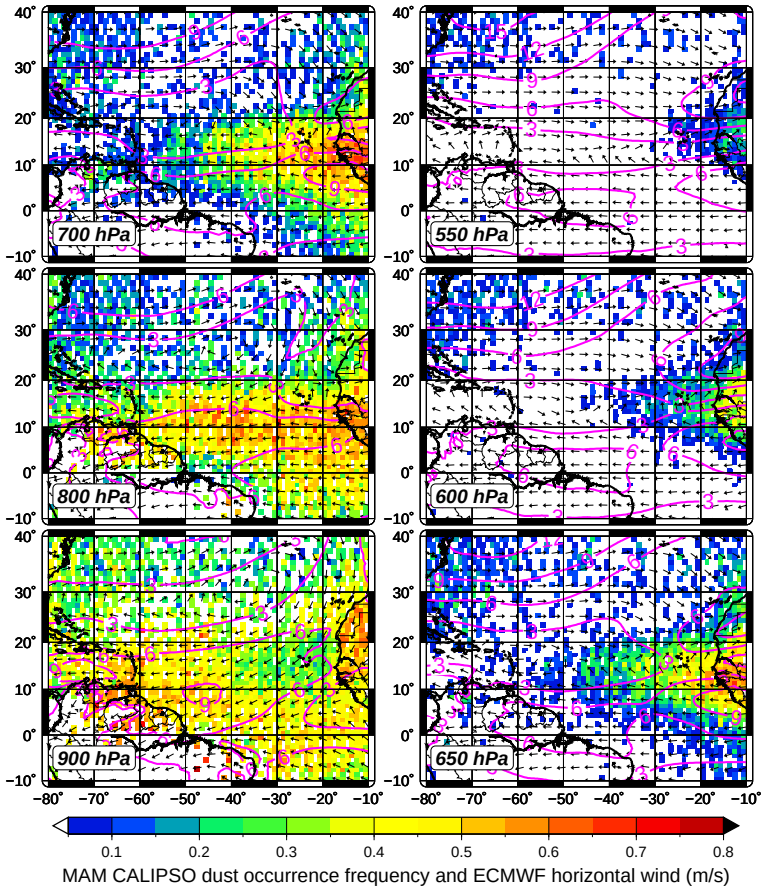

Fig. A2. Same as Fig. A1 but for spring (MAM).

ACPD
13, 4727–4784, 2013

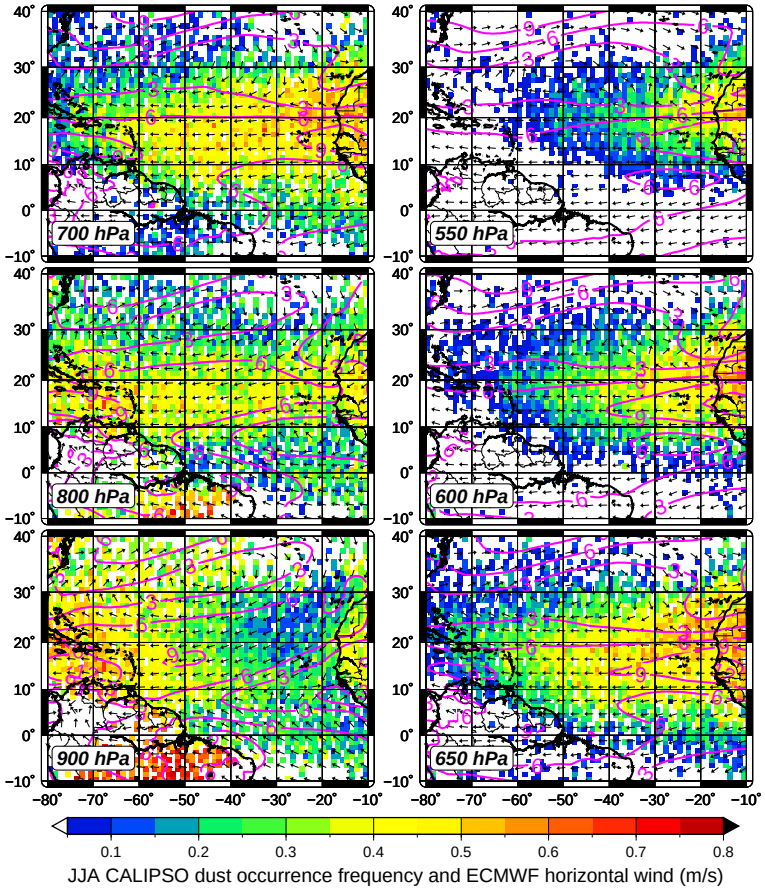

Fig. A3. Same as Fig. A1 but for summer (JJA).

ACPD
13, 4727–4784, 2013

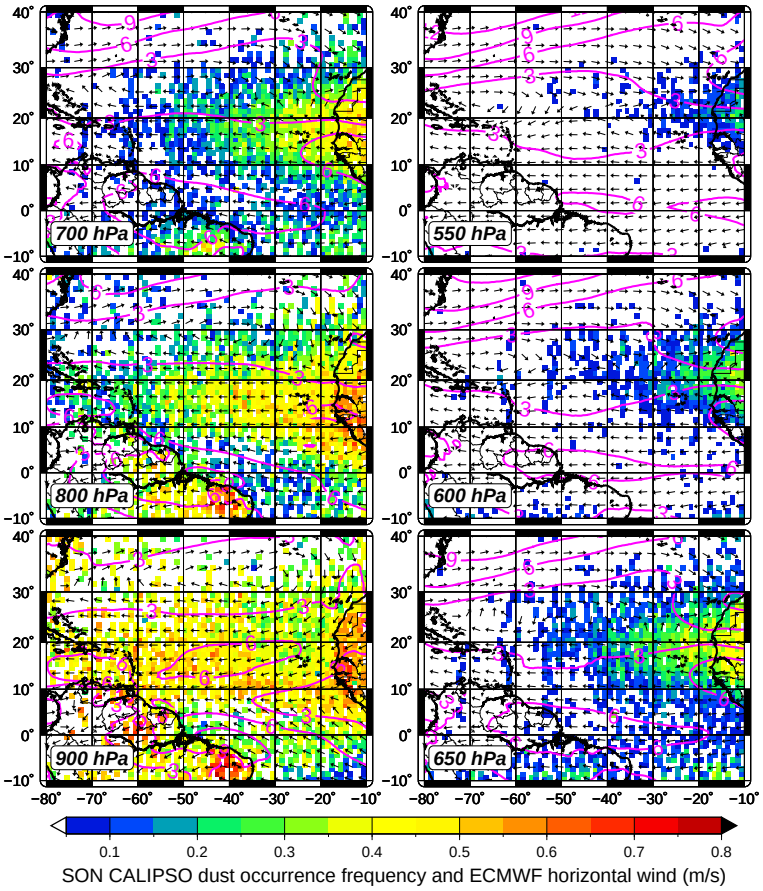

Fig. A4. Same as Fig. A1 but for fall (SON).

ACPD
13, 4727–4784, 2013